Deleterious variants in X-linked *CFAP47* induce asthenoteratozoospermia and primary male infertility

Chunyu Liu,[1,2,20] Chaofeng Tu,[3,4,5,20] Lingbo Wang,[1,2,6,20] Huan Wu,[7,8,9,20] Brendan J. Houston,[10,11] Francesco K. Mastrorosa,[12] Wen Zhang,[13] Ying Shen,[14] Jiaxiong Wang,[15,16] Shixiong Tian,[1,2] Lanlan Meng,[4] Jiangshan Cong,[1,2] Shenmin Yang,[15,16] Yiwen Jiang,[1] Shuyan Tang,[1,2] Yuyan Zeng,[1] Mingrong Lv,[7,8,9] Ge Lin,[3,4,5] Jinsong Li,[6] Hexige Saiyin,[1] Xiaojin He,[7,8,9] Li Jin,[1] Aminata Touré,[17] Pierre F. Ray,[17,18] Joris A. Veltman,[12] Qinghua Shi,[19,21] Moira K. O'Bryan,[10,11,21] Yunxia Cao,[7,8,9,21] Yue-Qiu Tan,[3,4,5,21,*] and Feng Zhang[1,2,21,*]

Summary

Asthenoteratozoospermia characterized by multiple morphological abnormalities of the flagella (MMAF) has been identified as a sub-type of male infertility. Recent progress has identified several MMAF-associated genes with an autosomal recessive inheritance in human affected individuals, but the etiology in approximately 40% of affected individuals remains unknown. Here, we conducted whole-exome sequencing (WES) and identified hemizygous missense variants in the X-linked *CFAP47* in three unrelated Chinese individuals with MMAF. These three *CFAP47* variants were absent in human control population genome databases and were predicted to be deleterious by multiple bioinformatic tools. *CFAP47* encodes a cilia- and flagella-associated protein that is highly expressed in testis. Immunoblotting and immunofluorescence assays revealed obviously reduced levels of CFAP47 in spermatozoa from all three men harboring deleterious missense variants of *CFAP47*. Furthermore, WES data from an additional cohort of severe asthenoteratozoospermic men originating from Australia permitted the identification of a hemizygous Xp21.1 deletion removing the entire *CFAP47* gene. All men harboring hemizygous *CFAP47* variants displayed typical MMAF phenotypes. We also generated a *Cfap47*-mutated mouse model, the adult males of which were sterile and presented with reduced sperm motility and abnormal flagellar morphology and movement. However, fertility could be rescued by the use of intra-cytoplasmic sperm injections (ICSIs). Altogether, our experimental observations in humans and mice demonstrate that hemizygous mutations in *CFAP47* can induce X-linked MMAF and asthenoteratozoospermia, for which good ICSI prognosis is suggested. These findings will provide important guidance for genetic counseling and assisted reproduction treatments.

Introduction

Infertility is a common medical condition affecting an estimated 15% of couples worldwide.[1] Males account for approximately 50% of infertile individuals, and the potential factors for male infertility are complex and diverse.[2] Asthenoteratozoospermia is the clinical descriptor used to describe men who produce sperm with abnormal morphology and reduced motility and encompasses a significant proportion of male infertility.[3]

Multiple morphological abnormalities of the flagella (MMAF) is a subtype of asthenoteratozoospermia proposed in 2014 and is characterized by the presence in the ejaculate of sperm with a combination of absent, short, coiled, bent, and/or irregular-caliber flagella.[4] Autosomal recessive inheritance has been suggested for many forms of human MMAF,

[1]Obstetrics and Gynecology Hospital, NHC Key Laboratory of Reproduction Regulation (Shanghai Institute of Planned Parenthood Research), State Key Laboratory of Genetic Engineering at School of Life Sciences, Fudan University, Shanghai 200011, China; [2]Shanghai Key Laboratory of Female Reproductive Endocrine Related Diseases, Shanghai 200011, China; [3]Institute of Reproductive and Stem Cell Engineering, School of Basic Medical Science, Central South University, Changsha 410000, China; [4]Reproductive and Genetic Hospital of CITIC-Xiangya, Changsha 410000, China; [5]Clinical Research Center for Reproduction and Genetics in Hunan Province, Changsha 410000, China; [6]State Key Laboratory of Cell Biology, Shanghai Key Laboratory of Molecular Andrology, CAS Center for Excellence in Molecular Cell Science, Shanghai Institute of Biochemistry and Cell Biology, Chinese Academy of Sciences, University of Chinese Academy of Sciences, Shanghai 200031, China; [7]Reproductive Medicine Center, Department of Obstetrics and Gynecology, The First Affiliated Hospital of Anhui Medical University, Hefei 230022, China; [8]NHC Key Laboratory of Study on Abnormal Gametes and Reproductive Tract, Anhui Medical University, Hefei 230032, China; [9]Key Laboratory of Population Health Across Life Cycle, Anhui Medical University, Ministry of Education of the People's Republic of China, Hefei 230032, China; [10]School of Biological Sciences, Monash University, Clayton, VIC 3800, Australia; [11]School of BioSciences, The University of Melbourne, Parkville, VIC 3010, Australia; [12]Biosciences Institute, Faculty of Medical Sciences, Newcastle University, NE2 4HH Newcastle upon Tyne, UK; [13]Fudan University Pudong Medical Center, Shanghai Key Laboratory of Medical Epigenetics, Institutes of Biomedical Sciences, Department of Systems Biology for Medicine, School of Basic Medical Sciences, Fudan University, Shanghai 200032, China; [14]Department of Obstetrics/Gynecology, Key Laboratory of Obstetric, Gynecologic and Pediatric Diseases and Birth Defects of Ministry of Education, West China Second University Hospital, Sichuan University, Chengdu 610041, China; [15]State Key Laboratory of Reproductive Medicine, The Affiliated Suzhou Hospital of Nanjing Medical University, Suzhou 215002, China; [16]Suzhou Municipal Hospital, Suzhou 215002, China; [17]Team Genetics Epigenetics and Therapies of Infertility, Institute for Advance Biosciences, Grenoble Alpes University, INSERM U1209, Centre National de la Recherche Scientifique UMR 5309, Grenoble 38000, France; [18]UM de genetique de l'infertilite et de diagnostic pre-implantatoire, Centre Hospitalier Universitaire Grenoble Alpes, Grenoble 38000, France; [19]The First Affiliated Hospital of USTC, Hefei National Laboratory for Physical Sciences at Microscale, CAS Key Laboratory of Innate Immunity and Chronic Disease, School of Basic Medical Sciences, Division of Life Sciences and Medicine, CAS Center for Excellence in Molecular Cell Science, Collaborative Innovation Center of Genetics and Development, University of Science and Technology of China, Hefei 230027, China
[20]These authors contributed equally to this work
[21]These authors contributed equally to this work
*Correspondence: tanyueqiu@csu.edu.cn (Y.-Q.T.), zhangfeng@fudan.edu.cn (F.Z.)
https://doi.org/10.1016/j.ajhg.2021.01.002.

and to date, 22 autosomal MMAF-associated genes have been identified: *AK7* (MIM: 615364), *ARMC2* (MIM: 618424), *CEP135* (MIM: 611423), *CFAP43* (MIM: 617558), *CFAP44* (MIM: 617559), *CFAP58* (MIM: 619129), *CFAP65* (MIM: 614270), *CFAP69* (MIM: 617949), *CFAP70* (MIM: 618661), *CFAP91* (MIM: 609910), *CFAP251* (MIM: 618146), *DNAH1* (MIM: 603332), *DNAH2* (MIM: 603333), *DNAH6* (MIM: 603336), *DNAH8* (MIM: 603337), *DNAH17* (MIM: 610063), *DZIP1* (MIM: 608671), *FSIP2* (MIM: 618153), *QRICH2* (MIM: 618304), *SPEF2* (MIM: 610172), *TTC21A* (MIM: 611430), and *TTC29* (MIM: 618735).[5–9] Yet there are still many individuals with MMAF that cannot be causally diagnosed, indicating the potential involvement of other genetic factors.

Sex chromosomes display important roles in sex determination and fertility. Previous studies indicated that many genes specifically or preferentially expressed in the testis are enriched on sex chromosomes.[10,11] Thus, deleterious mutations in these genes may have a direct phenotypic effect on male fertility because of the lack of the second compensatory X or Y allele.[12] Although the roles of Y chromosomal microdeletions in male infertility have been well understood,[13] only a few X-linked genes have been found to be associated with infertile phenotypes. For example, hemizygous *TEX11* (MIM: 300311) mutations were shown to cause meiotic arrest and azoospermia and hemizygous *ADGRG2* (MIM: 300572) mutations led to obstructive azoospermia in a large Pakistani family.[14,15]

In this study, we identified hemizygous deleterious variants of X-linked *CFAP47* (also known as *CXorf22*) in four unrelated men displaying asthenoteratozoospermia. Furthermore, an X-linked *Cfap47*-mutated mouse model was generated with CRISPR-Cas9 technology, and the adult males with a hemizygous *Cfap47* mutation were sterile and also displayed reduced sperm motility and abnormal flagella. Intra-cytoplasmic sperm injection (ICSI) treatment led to successful fertilization using the spermatozoa from *Cfap47*-mutated male mice and three of the four men harboring hemizygous *CFAP47* variants. All these findings indicate that X-linked *CFAP47* mutations are an important pathogenic factor of MMAF and asthenoteratozoospermia.

Material and methods

Human subjects

The initial two Chinese cohorts were composed of 243 MMAF-affected Chinese men recruited from the Reproductive and Genetic Hospital of CITIC-Xiangya (Changsha, China) and 88 MMAF-affected individuals recruited from the First Affiliated Hospital of Anhui Medical University (Hefei, China). The third cohort comprised 24 individuals with asthenoteratozoospermia enrolled in Australia. The clinical phenotypes of the affected individuals are described in the supplemental information (see Supplemental note). The study regarding the cohorts was approved by the institutional review boards at all the participating institutes, and signed informed consents were obtained from all subjects participating in the study.

Whole-exome sequencing

Genomic DNA was isolated from peripheral blood samples of human subjects via a DNeasy Blood and Tissue Kit (QIAGEN, 51106). Whole-exome sequencing (WES) analysis was performed on MMAF-affected subjects as previously described.[16,17] Briefly, we used 1 μg of genomic DNA to enrich the human exome by using the Agilent SureSelect Human All Exon V6 Kit or Twist Bioscience's Human Core Exome Kit and sequenced this on the HiSeq 2000 or NovaSeq 6000 sequencing platforms (Illumina). The obtained data were mapped to the human genome reference assembly (GRCh37/hg19) by the Burrows-Wheeler Aligner (BWA) software,[18] and PCR duplicates were marked and removed via the Picard software. Then ANNOVAR software was used for functional annotation with information from a variety of databases and bioinformatic tools, including OMIM, Gene Ontology, SIFT, PolyPhen-2, 1000 Genomes Project, and gnomAD.[19–23] Deleterious missense variants were predicted simultaneously via SIFT, PolyPhen-2, CADD, and/or M-CAP. Sanger sequencing was conducted for variant verification with the primers listed in Table S1.

Structural modeling for CFAP47 and its mutants

The mutants Ser1742Gly and Ile2385Asn of CFAP47 are located near the Pfam or CDD motifs, hence their effect on protein structure could be modeled with homology models. The structures with homology domains near the mutants Ser1742Gly and Ile2385Asn were modeled by SWISS-MODEL. The putative homology model for the proline rich peptide (Tyr2884-Gln2905) was also built for analysis on the basis of similar proline rich templates searched by SWISS-MODEL. Furthermore, the molecular dynamics (MD) simulation of this peptide was performed by UCSF Chimera with default settings. The major clusters of simulated structures were compared with original model (one cluster comparison was displayed). In addition, we also used the online tool HOPE[24] to further predict the potential effects of *CFAP47* missense variants on the structure of CFAP47.

Detection and validation of genomic copy number variations

Copy number variation (CNV) calling was performed with a custom GATK4-based pipeline. This workflow exploits the GATK4 sequence read-depth normalization[25] and a custom R-based segmentation and visualization.[26] The detected CNVs were annotated with AnnotSV.[27] All the CNVs present in more than 1% of the samples of the Database of Genomic Variations (DGV) were excluded. The remaining rare deletions and duplications were individually inspected through the genomic profiles and detailed Log_2Ratio plots generated by the workflow. Manual inspection of these plots allowed for distinguishing possible CNVs from background noise, and only CNVs involving more than two exons were considered for further validation.

The detected deletion was validated with a PCR assay. We designed three primer pairs to amplify the region encompassed by the deletion, while we designed three other primer pairs to amplify the closest gene outside the predicted breakpoints (Table S2 and Figure S1). The assay was conducted on the MMAF-affected subject MA2603 II-1 and male and female control individuals.

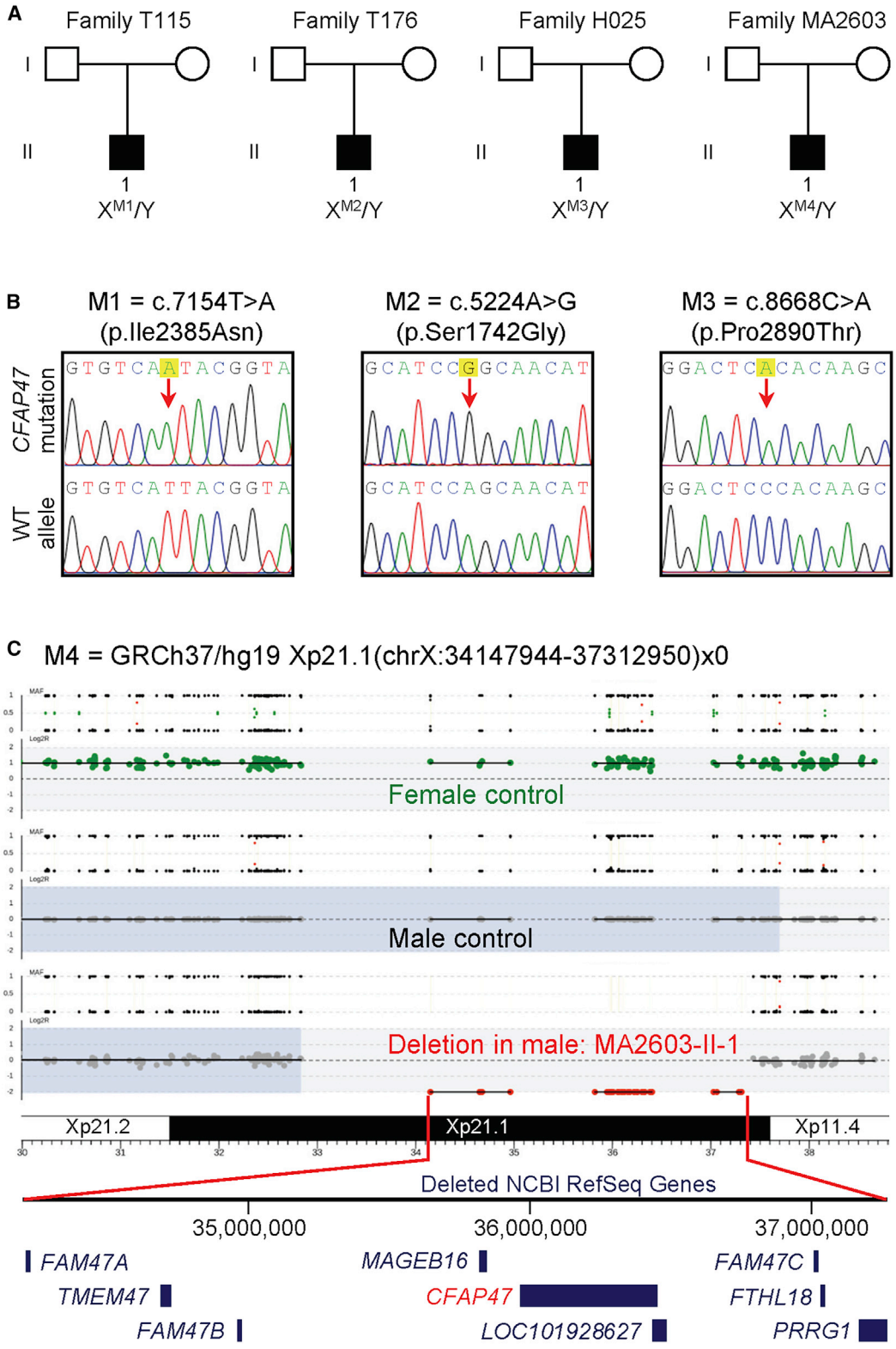

Figure 1. Identification of hemizygous variants of X-linked *CFAP47* in men with asthenoteratozoospermia
(A) Pedigrees of four families affected by hemizygous *CFAP47* variants (M1–M4). Black filled squares indicate the male individuals with asthenoteratozoospermia.
(B) Sanger sequencing confirmed hemizygous *CFAP47* missense variants (M1–M3) in subjects T115 II-1, T176 II-1, and H025 II-1, respectively. The positions of variants are indicated by red arrows. WT, wild type.
(C) An approximately 3.2-Mb Xp21.1 deletion affecting *CFAP47* (M4) in subject MA2603 II-1. This hemizygous deletion removed the entire *CFAP47* gene copy.

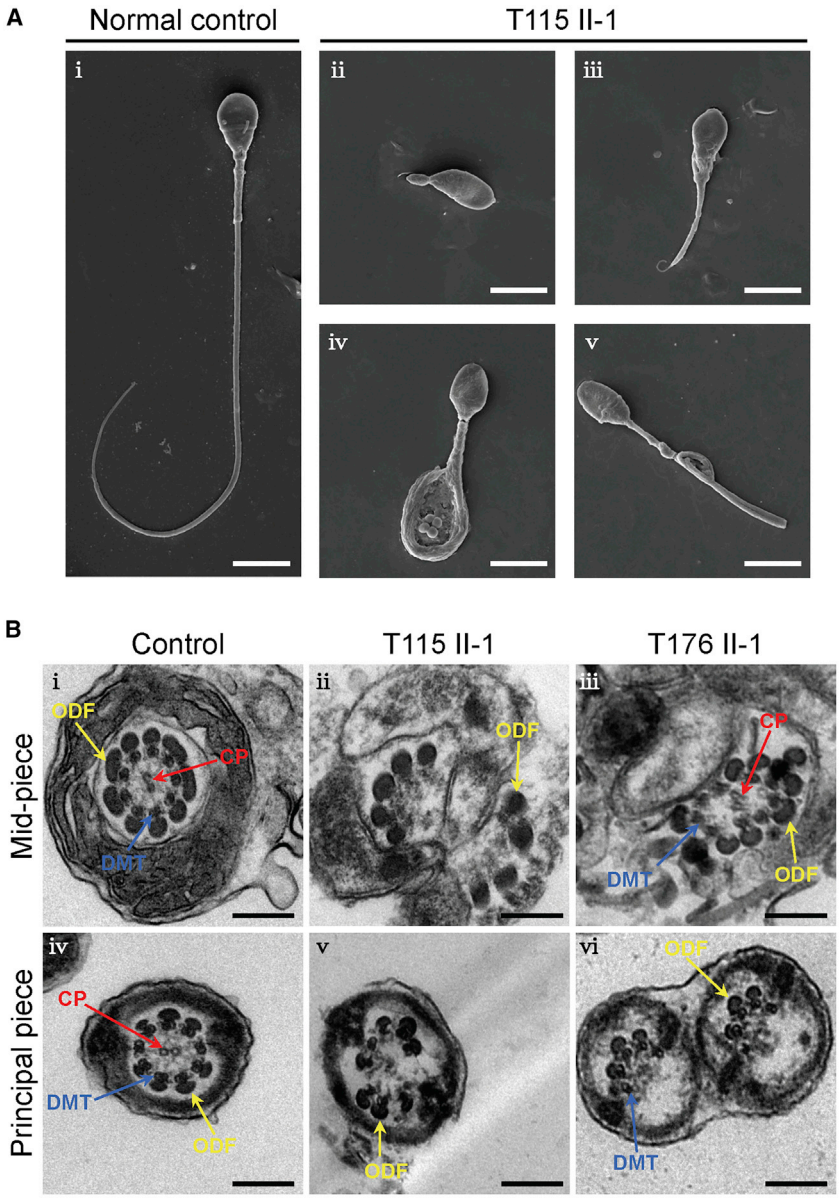

Figure 2. Sperm morphology and ultrastructure analyses for men harboring hemizygous *CFAP47* variants

(A) SEM analysis of the spermatozoa from a male control individual and men harboring hemizygous *CFAP47* variants. (i) Normal morphology of the spermatozoon from a healthy control male. (ii–v) Most spermatozoa from men harboring hemizygous *CFAP47* variants displayed typical MMAF phenotypes, including absent (ii), short (iii), coiled (iv), and bent flagella (v). The data of subject T115 II-1 were shown as an example. Scale bars: 5 μm.

(B) TEM analysis of the spermatozoa from a male control individual and men harboring hemizygous *CFAP47* variants. Cross-sections of the midpiece (i) and principal piece (iv) of the sperm flagella from a male control individual displayed typical "9+2" microtubule structure: the central pair of microtubules (CP; red arrows) and nine pairs of peripheral microtubule doublets (DMTs; blue arrows) surrounded by nine outer dense fibers (ODFs; yellow arrows). The organized mitochondrial sheath and fibrous sheath are also observed. Cross-sections of the spermatozoa from men harboring hemizygous *CFAP47* variants revealed various axonemal anomalies, including misarranged ODFs (ii, iii) and missing DMTs and/or the CP (v and vi). Scale bars: 200 nm.

Semen parameter analysis

Semen samples of human subjects were collected through masturbation after 2–7 days of sexual abstinence and analyzed in the source laboratories as part of the routine biological examination according to the 5th World Health Organization (WHO) guidelines. The morphology of the sperm cells was assessed with hematoxylin and eosin (H&E) staining and scanning electron microscopy (SEM). The morphological abnormalities of sperm flagella were classified into five categories: absent, short, bent, coiled flagella, and flagella of irregular caliber.[4] We examined at least 200 spermatozoa for each subject to evaluate the percentages of morphologically abnormal spermatozoa.

For sperm morphology and motility analyses of the mouse model, spermatozoa were extracted from the caput, corpus, and cauda epididymides through dissection of adult male mice and diluted in 1 mL human tubal fluid (HTF; Millipore, Cat. # MR-070-D) for 15 min at 37°C. Sperm morphology was analyzed by H&E staining and/or SEM, and sperm motility was further assessed with the spermatozoa from cauda epididymides by a computer-assisted sperm analysis (CASA) system.

Electron microscopy evaluation

For electron microscopy evaluation, semen samples were prepared as previously described.[28] In brief, for SEM assay, sperm specimens were deposited on poly-L-lysine-coated coverslips, fixed in 2.5% glutaraldehyde, washed in 0.1 mol/L phosphate buffer, and post-fixed in osmic acid. The specimens were then progressively dehydrated with ethanol and isoamyl acetate gradient, then dried with a CO_2 critical-point dryer (Eiko HCP-2, Hitachi). Next, the specimens were mounted on aluminum stubs, sputter coated by use of an ionic sprayer meter (Eiko E-1020, Hitachi), and analyzed via SEM (Stereoscan 260) under an accelerating voltage of 20 kV.

For transmission electron microscopy (TEM), semen samples were rinsed and immersed routinely and then were progressively dehydrated with graded ethanol (50%, 70%, 90%, and 100%) and 100% acetone, followed by infiltration with 1:1 acetone and SPI-Chem resin overnight at 37°C. After being embedded in Epon 812, the specimens were sliced with ultra-microtome, stained with uranyl acetate and lead citrate, and observed and photographed via TEM (TECNAI-10, Philips) with an accelerating voltage of 80 kV. For TEM analysis of mouse sperm, cauda epididymis samples were prepared as described previously.[16]

Table 1. Hemizygous deleterious *CFAP47* variants identified in Chinese MMAF-affected men

CFAP47 variant	M1	M2	M3
cDNA alteration	c.7154T>A	c.5224A>G	c.8668C>A
Variant allele	hemizygous	hemizygous	hemizygous
Protein alteration	p.Ile2385Asn	p.Ser1742Gly	p.Pro2890Thr
Variant type	missense	missense	missense
Allele frequency in human population			
1000 Genomes Project	0	0	0
East Asians in gnomAD	0	0	0
All individuals in gnomAD	0	0	0
Function prediction			
SIFT	damaging	damaging	damaging
PolyPhen-2	damaging	N/A	damaging
M-CAP	N/A	damaging	damaging
CADD	8.6	23.4	23.1

NCBI reference sequence number of *CFAP47* is GenBank: NM_001304548.2. Variants with CADD values greater than 4 are considered to be deleterious. N/A, not available.

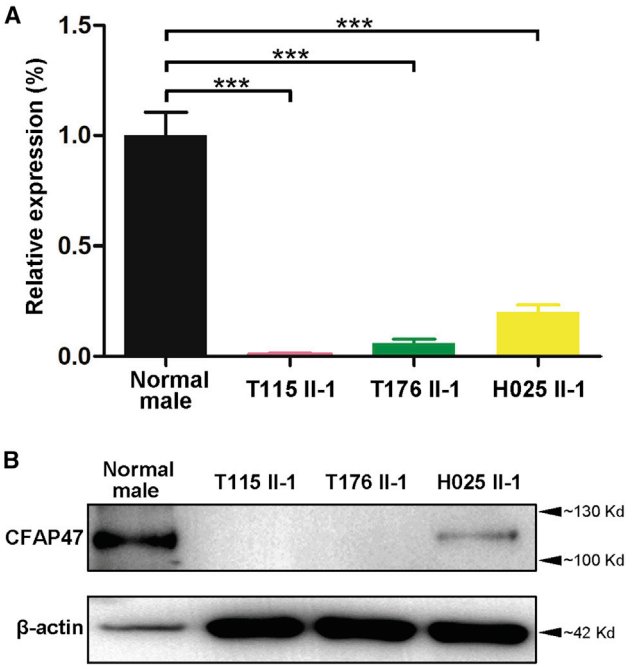

Figure 3. Expression analysis of *CFAP47* mRNA and CFAP47 in the spermatozoa from a male control individual and men harboring hemizygous *CFAP47* variants

(A) Real-time quantitative PCR analysis indicated that the abundance of *CFAP47* mRNA was dramatically reduced in the sperm from men harboring hemizygous *CFAP47* variants when compared to that of a control male. Data represent the means ± standard error of measurement of three independent experiments. Two-tailed Student's paired or unpaired t tests were used as appropriate (***$p < 0.001$).

(B) Immunoblotting assay revealed that CFAP47 was dramatically reduced or nearly absent in the spermatozoa from men harboring *CFAP47* mutations. β-actin was used as a loading control.

Mouse model generation

Cfap47-mutated mice were generated with CRISPR-Cas9 technology. Cas9 and sgRNA were prepared as previously described.[29] The CRISPR-Cas9 reagents were directly injected into zygotes of C57BL/6 mice. After injection, the zygotes were further cultured in KSOM medium (Millipore, Cat. # MR-106-D) at 37°C under 5% CO_2 to reach the 2-cell stage, followed by embryo transfer into oviducts of female pseudopregnant Institute of Cancer Research (ICR) mice at 0.5 days post-coitum (dpc). We used PCR assay and Sanger sequencing to identify the frameshift mutation in founder mice (Table S3). Adult mice (aged 7 weeks or older) were used in this study. All animal experiments were carried out in accordance with the recommendations of the US National Institutes of Health's Guide for the Care and Use of Laboratory Animals. The study was approved by the animal ethics committee at the School of Life Sciences of Fudan University.

Real-time quantitative PCR and reverse-transcription PCR

For real-time quantitative PCR, total RNAs of human spermatozoa and mouse testes were extracted with the Allprep DNA/RNA/Protein Mini Kit (QIAGEN). Approximately 1 μg of obtained RNA was converted into cDNA with HiScript II Q RT SuperMix for quantitative PCR (Vazyme). The obtained cDNA was individually diluted 5-fold to be used as templates for the subsequent real-time quantitative PCR with AceQ quantitative PCR SYBR Green Master Mix (Vazyme) on a CFX Connect Real-Time PCR Detection System. *GAPDH*/*Gapdh* was used as an internal control, and primers for real-time quantitative PCR are listed in Table S4.

For reverse-transcription PCR (RT-PCR), total RNAs of various tissues of adult C57BL/6N mice were extracted and reverse transcribed as described above. RT-PCR was performed with 10 ng of cDNA, and *Hprt* was used as an internal control (Figure S2 and Table S4).

Immunoblotting

The proteins of human sperm cells were extracted via Minute Total Protein Extraction Kit for Animal Cultured Cells and Tissues (Invent) then denatured at 95°C for 10 min. The denatured proteins were separated by 10% sodium dodecyl sulfate polyacrylamide gel electrophoresis (SDS-PAGE) and transferred onto polyvinylidene difluoride (PVDF) membrane (Millipore). Membranes were blocked in 5% non-fat milk for 1 h at room temperature before incubation overnight at 4°C with the following primary antibodies: rabbit polyclonal anti-CXorf22 (i.e., anti-CFAP47; GTX80633, GeneTex, 1:1000) and HRP-conjugated beta actin (HRP-60008, Proteintech, 1:2000). The membranes were then washed in TBST (Tris-buffered saline with Tween-20) three times and incubated with HRP-conjugated anti-Rabbit IgG antibody (Abmart, M21002) at a 1:2500 dilution in blocking solution for 1 h at room temperature. We used the Chemistar High-sig ECL Western Blotting Substrate (Tanon) to detect immunoreactive protein bands by Tanon 5200.

Immunoprecipitations

For immunoprecipitations, proteins were extracted from the sperm cells of a control man and the testes of adult wild-type mice and incubated with 5 μg of a customized CFAP65 antibody (Abclonal, China, specifically binding the amino acids 1401–1635 of mouse Cfap65) overnight at 4°C. Next, 50 μL of Protein

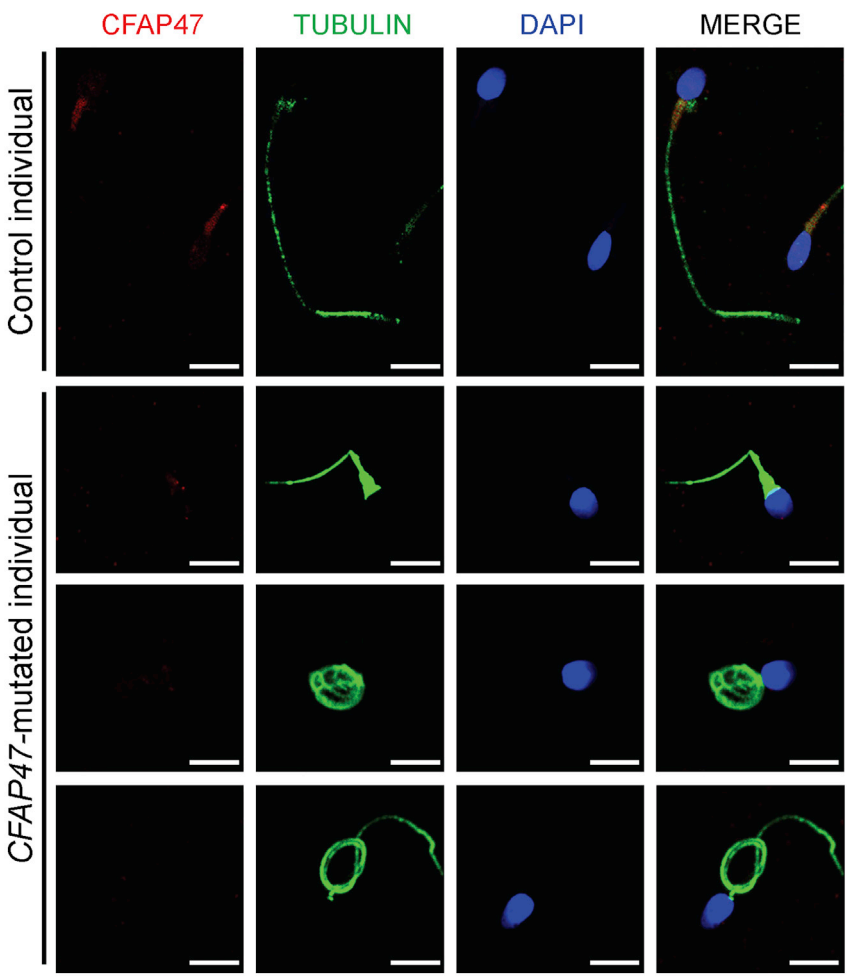

Figure 4. Immunofluorescence staining of CFAP47 in the spermatozoa from a male control individual and men harboring hemizygous *CFAP47* variants

Sperm cells were stained with anti-CFAP47 (red) and anti-α-tubulin (green) antibodies. DNA was counterstained with DAPI (4′,6-diamidino-2-phenylindole) as a marker of the cell nucleus. CFAP47 staining is concentrated at the base of sperm flagella from the control individual, but the signal was almost absent in the sperm flagella from men harboring hemizygous *CFAP47* variants. Scale bars: 5 μm.

A/G Magnetic Beads (Pierce Biotechnology, Rockford, IL, USA) was added to each incubation sample for 1 h at room temperature on a rotating mixer. The beads were then washed three times with the manufacturer's immunoprecipitation lysis and wash buffer. Finally, the co-immunoprecipitated proteins were analyzed by immunoblotting with CFAP65 (diluted at 1:1000) and CXorf22 (i.e., CFAP47; diluted at 1:1000) antibodies.

Immunofluorescence analysis

For immunofluorescence localization of proteins, sperm cells obtained from human MMAF-affected individuals and control subjects were washed in phosphate-buffered saline (PBS), fixed in 4% paraformaldehyde for 30 min at room temperature, and coated on the slides treated with 0.1% poly-L-lysine pre-coated slides (Thermo Fisher). Non-specific antibody binding was blocked in 10% donkey serum for 1 h at room temperature, and sperm were incubated overnight at 4°C with the following primary antibodies: rabbit polyclonal anti-CXorf22 (GTX80633, GeneTex, 1:100), anti-CFAP65 (CSB-PA757963LA01HU, CUSABIO, 1:100), anti-SPAG16 (PA5-57995, Invitrogen, 1:100), and monoclonal mouse anti-α-tubulin (T9026, Sigma, 1:500). Next, the slides were washed with PBS with 0.1% (v/v) Tween-20 before 1 h incubation at room temperature with the highly cross-absorbed secondary antibodies Alexa Fluor 488 anti-Mouse IgG (34106ES60, Yeasen, 1:1000) and Cy3-conjugated AffiniPure Goat Anti-Rabbit IgG (111-165-003, Jackson, 1:4000). The images were captured with a confocal microscope (Zeiss LSM 880).

In vitro fertilization and ICSI in mice

In vitro fertilization (IVF) and ICSI analyses in mice were conducted as previously described.[17] In brief, the wild-type female mice were superovulated by injection of 5–7.5 IU of pregnant mare serum gonadotropin (PMSG), followed by 5–7.5 IU of human chorionic gonadotropin (hCG) 48 h later. For IVF, sperm samples collected from mouse cauda epididymides were added into the HTF drop. Next, cumulus-intact oocytes collected from superovulated female mice were transferred into the sperm-containing HTF drop. After incubation for 5–6 h, mouse embryos were washed in HTF and transferred into KSOM medium (Millipore, Cat. # MR-106-D) for further culture (37°C, 5% CO_2). We then evaluated fertilization rates by recording the numbers of two-cell embryos and late-stage blastocysts at 20 h and 91 h later, respectively. For ICSI, mouse sperm heads were separated from sperm tails and injected into mouse oocytes obtained from superovulated females by a Piezo driven pipette as previously described.[30] Then the injected oocytes were cultured in KSOM medium at 37°C under 5% CO_2. Two-cell embryos and blastocysts were counted 20 h and 96 h later, respectively.

Results

Identification of rare and hemizygous *CFAP47* variants in men with asthenoteratozoospermia

In this study, we combined SNV and CNV calling from WES data to identify potential candidate genes associated with MMAF. Hemizygous missense variants of X-linked *CFAP47* were initially identified in three Chinese MMAF-affected individuals from unrelated families in the Chinese cohorts: c.7154T>A (p.Ile2385Asn) in subject T115 II-1, c.5224A>G (p.Ser1742Gly) in subject T176 II-1, and c.8668C>A (p.Pro2890Thr) in subject H025 II-1 (Figures 1A, 1B, and 2 and Table 1). These hemizygous *CFAP47* variants were absent in the human population genome

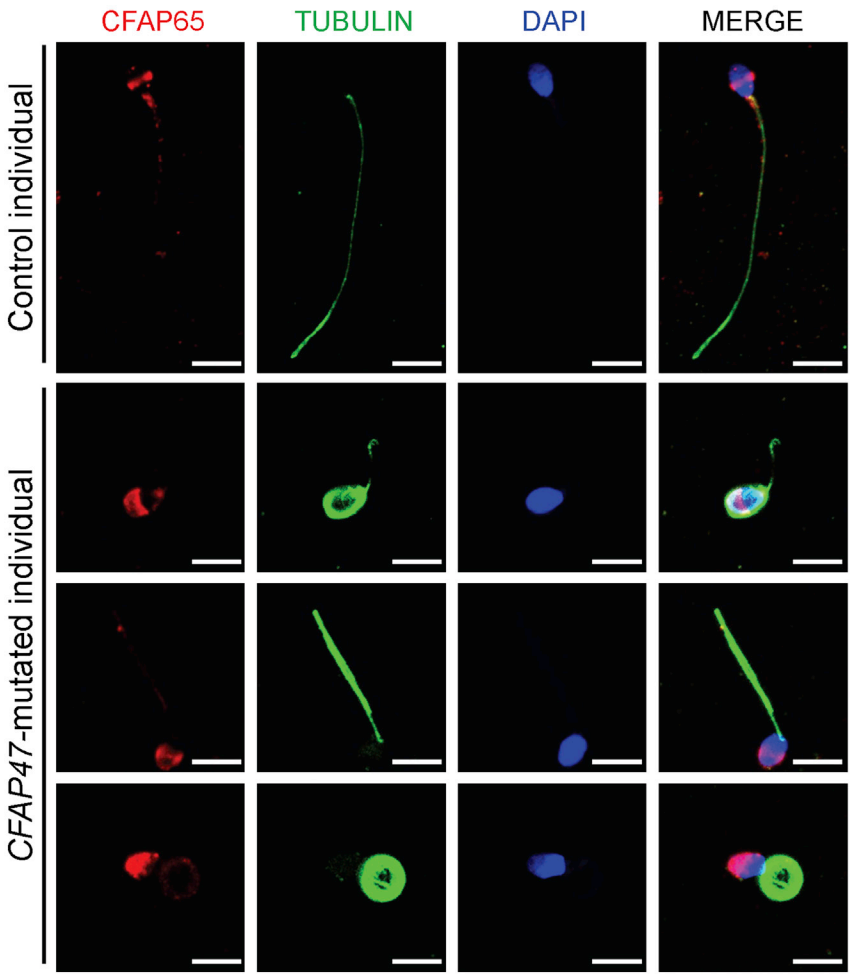

Figure 5. Abnormal CFAP65 location in the spermatozoa from men harboring hemizygous *CFAP47* variants

Sperm cells were stained with anti-CFAP65 (red) and anti-α-tubulin (green) antibodies. DNA was counterstained with DAPI as a marker of the cell nucleus. CFAP65 staining was observed mainly at the equatorial segment of sperm head and the base of flagella in control spermatozoa, but the signal was only diffusely clustered in the acrosome of spermatozoa from men harboring hemizygous *CFAP47* variants. Scale bars: 5 μm.

datasets, including 1000 Genomes Project and gnomAD (v2.1.1 with 141,456 samples) (Table 1). All these *CFAP47* missense variants were predicted to be deleterious through utilization of the PolyPhen-2, SIFT, CADD, and M-CAP tools (Table 1).

CFAP47 (formerly known as *CXorf22*, GenBank: NM_001304548.2) is located on the human chromosome X and highly expressed in the testis. *CFAP47* encodes a cilia- and flagella-associated protein. The residues in CFAP47 affected by *CFAP47* missense variants p.Ile2385Asn (subject T115 II-1), p.Ser1742Gly (subject T176 II-1), and p.Pro2890Thr (subject H025 II-1) are all highly conserved across species (Figure S3). Further analysis of protein structural modeling via online bioinformatic tools revealed the severe effects of these amino acid-substituting mutations on the structure and/or stability of CFAP47. These included changes in the hydrophobicity in CFAP47 mutant p.Ile2385Asn, the structure flexibility in CFAP47 mutant p.Ser1742Gly, and backbone flexibility or residue charge in CFAP47 mutant p.Pro2890Thr. These findings indicated the potential contribution of these *CFAP47* missense variants to MMAF (Figure S4 and Table S5).

Furthermore, CNV calling from WES data permitted the identification of a hemizygous Xp21.1 deletion eliminating the entire *CFAP47* in subject MA2603 II-1 from the Australian cohort (Figure 1C). PCR analysis with primer pairs for the region encompassed by the deletion and outside the predicted breakpoints further confirmed the deletion segment (Figure S1). No genic or exonic deletions of *CFAP47* were reported in either DGV (14,316 samples) or gnomAD-SV (v2.1 with 10,847 samples). These findings further suggest the involvement of deleterious *CFAP47* variants in MMAF across human populations.

Deficiency of CFAP47 and its association with CFAP65

To investigate the pathogenicity of the *CFAP47* variants identified in this study, we analyzed the expression of *CFAP47* mRNA and protein in the sperm samples from a fertile control individual and the men harboring hemizygous *CFAP47* variants. Real-time quantitative PCR assays suggested that the abundances of *CFAP47* mRNA were significantly reduced in the spermatozoa from men harboring hemizygous *CFAP47* variants (Figure 3A). Consistently, as shown by immunoblotting and immunostaining assays, the signal of CFAP47 was dramatically reduced, or absent, in the spermatozoa from men harboring hemizygous *CFAP47* variants (Figures 3B and 4). Thus, MMAF phenotypes described in this study were most likely caused by hemizygous deleterious variants in *CFAP47*.

Previous studies have reported that the deficiency of another cilia- and flagella-associated protein, CFAP65, can cause male infertility with MMAF.[28,31–33] Furthermore, STRING analysis indicates that CFAP47 may be highly connected with CFAP65 (Figure S5). To investigate the potential association between these two proteins, we performed immunostaining assay by using a commercial antibody against CFAP65 on the spermatozoa from men harboring hemizygous *CFAP47* variants. We observed that CFAP65 immunostaining was localized mainly at the equatorial segment of sperm head and the base of flagella in normal

Table 2. Semen characteristics and sperm morphology in men harboring hemizygous *CFAP47* variants

Subject	T115 II-1	T176 II-1	H025 II-1	MA2603 II-1	Reference limits
Semen parameter					
Semen volume (mL)	4.0	0.9	5.2	5.6	1.5[a]
Sperm concentration (10^6/mL)	2.5	3.0	29.5	0.5	15.0[a]
Motility (%)	18.9	14.3	23.3	10.0	40.0[a]
Progressive motility (%)	7.1	8.1	18.5	5.0	32.0[a]
Sperm morphology					
Absent flagella (%)	37.5	11.0	22.0	N/A	5.0[b]
Short flagella (%)	34.0	17.0	14.0	N/A	1.0[b]
Coiled flagella (%)	18.5	42.0	50.5	N/A	17.0[b]
Angulation (%)	3.5	5.0	2.0	N/A	13.0[b]
Irregular caliber (%)	6.5	6.5	3.5	N/A	2.0[b]

N/A, not available.
[a]Reference limits according to the WHO standards.[35]
[b]Reference limits according to the distribution range of morphologically normal spermatozoa observed in 926 fertile individuals.[36]

spermatozoa from control individuals, whereas the CFAP65 signal was only diffusely clustered in the acrosome of spermatozoa from MMAF-affected individuals harboring hemizygous *CFAP47* variants (Figure 5). Importantly, the abnormal location of CFAP65 was not observed in sperm cells from MMAF-affected individuals with other genetic defects such as bi-allelic mutations in *DNAH8*, *SPEF2*, or *CFAP58* (Figure S6). In addition, sperm cells from men harboring bi-allelic *CFAP65* variants displayed a significantly reduced CFAP47 staining when compared with the obvious CFAP47 signal in the mid-piece of flagella in normal spermatozoa (Figure S7). Consistently, obvious CFAP47/Cfap47 signals were also observed when we immunoprecipitated CFAP65/Cfap65 from human spermatozoa or mouse testis lysates and immunoblotted with CFAP47/Cfap47 antibodies (Figure S8). These findings collectively confirm a potential interaction and/or inter-regulation between CFAP65 and CFAP47 during spermiogenesis.

Asthenoteratozoospermia phenotypes in men harboring hemizygous *CFAP47* variants

Semen parameters of men harboring hemizygous *CFAP47* variants were acquired from the source laboratories during routine examination of the individuals according to WHO guidelines.[34] A semen analysis indicated the severely reduced sperm motility in all of four men harboring hemizygous *CFAP47* variants (Table 2). Furthermore, the rates of sperm progressive motility were dramatically decreased in men harboring hemizygous *CFAP47* variants (Table 2). Sperm morphological study was conducted by H&E staining and SEM. In comparison to long and thin tails of the sperm obtained from a fertile control man, the spermatozoa from men harboring hemizygous *CFAP47* variants displayed frequently abnormal flagella, including absent, short, coiled flagella, and irregular caliber (Figure 2A and Table 2).

We further conducted TEM to investigate sperm flagellar ultrastructure in the two Chinese men harboring hemizygous *CFAP47* variants. In contrast to typical "9+2" axoneme microtubule structure in the sperm flagella from a control specimen, the sperm flagella of men harboring hemizygous *CFAP47* variants displayed a variety of ultrastructural defects, including disorganization of outer dense fibers, and absence of peripheral or central microtubules at the midpiece and principal piece of sperm flagella (Figure 2B). In addition, the deficiency of SPAG16 (a component of core axoneme complex) was revealed, further suggesting the defect of core axoneme in the sperm flagella from men harboring hemizygous *CFAP47* variants (Figure S9).

Asthenoteratozoospermia phenotypes in *Cfap47*-mutated male mice

As shown in Figure S3, CFAP47 is conserved among mammalian species. Our RT-PCR assays using various mouse tissues indicated the preferential expression of mouse *Cfap47* (also located on the X chromosome) in the testis (Figure S2). To further investigate the role of mouse CFAP47 in sperm flagellar formation, we constructed *Cfap47*-mutated mice by using the CRISPR-Cas9 system (Figure S10A). Sanger sequencing of *Cfap47*-mutated male mice (*Cfap47*$^{-}$/Y) confirmed the presence of a hemizygous frameshift mutation (c.2559insT), which was predicted to cause premature translational termination (p.Gly855Profs*8) (Figure S10B). Real-time quantitative PCR assays showed that the abundance of *Cfap47* mRNA was significantly reduced in the spermatozoa from *Cfap47*$^{-}$/Y male mice when compared with wild-type male (*Cfap47*$^{+}$/Y) controls (Figure S11A). Consistently, immunostaining analysis performed with CFAP47 antibody revealed that CFAP47 staining was mainly located at the mid-piece of sperm flagella from wild-type male mice, but CFAP47 signal was almost absent in the spermatozoa from *Cfap47*-mutated male mice (Figure S11B).

Sperm morphology and parameters, together with flagellar ultra-structure, were also investigated in *Cfap47*-mutated male mice. Notably, diminished and abnormal sperm movements (a "folding" motion) were observed in *Cfap47*-mutated mice (Videos S1 and S2). CASA analyses indicated that both total sperm motility and progressive motility were significantly reduced in *Cfap47*-mutated male mice when compared to those of wild-type male mice (Figures 6A and 6B and Table S6). Furthermore, the rates of immotile and non-progressive spermatozoa from *Cfap47*-mutated male mice were significantly higher than

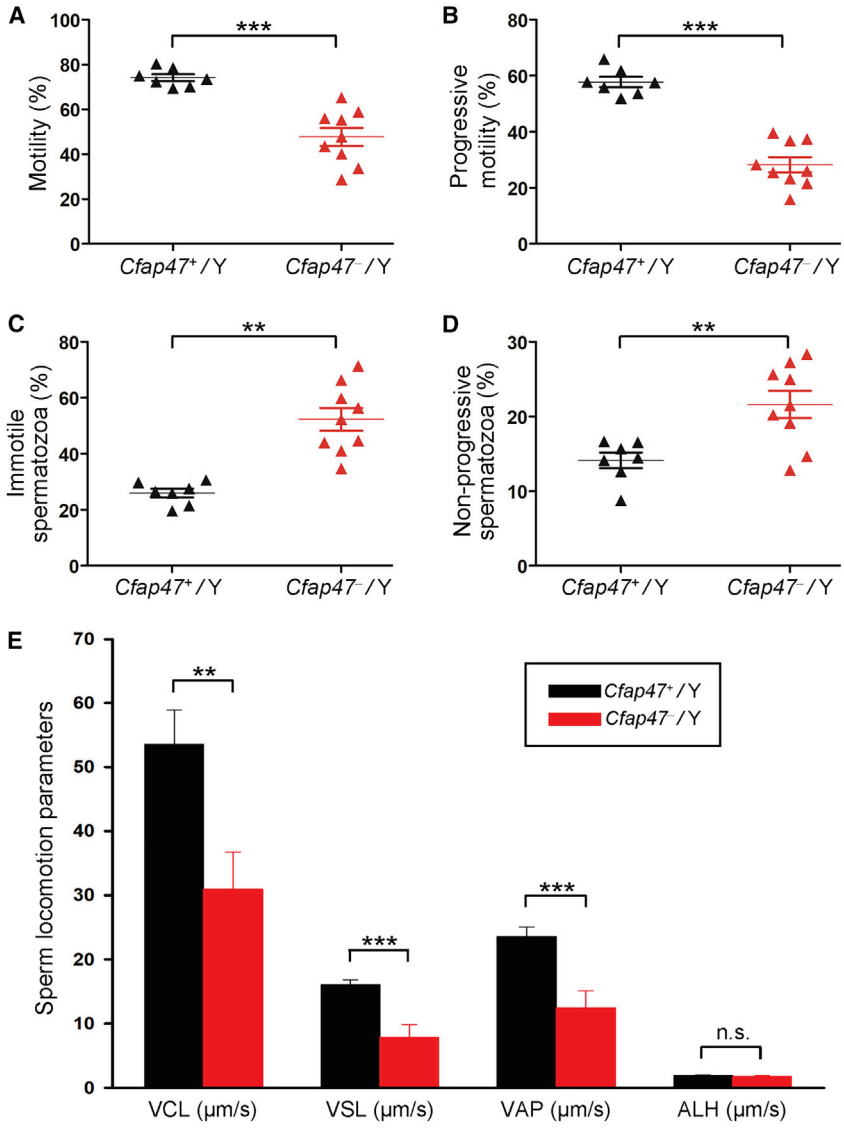

Figure 6. Semen characteristics of *Cfap47*-mutated male mice

(A–D) Semen characteristics by computer-assisted analysis system revealed significantly lower rates of sperm motility (A) and progressive motility (B) but significantly higher rates of immotile spermatozoa (C) and non-progressive spermatozoa (D) in *Cfap47*-mutated (*Cfap47*$^{-}$/Y) male mice when compared with those in wild-type (*Cfap47*$^{+}$/Y) male mice. (E) Curvilinear velocity (VCL), straight-line velocity (VSL), and average-path velocity (VAP) were also dramatically reduced in *Cfap47*-mutated male mice. Error bars represent the standard error of the mean. **$p < 0.01$; ***$p < 0.001$; n.s., not significant (Student's t test). ALH, amplitude of lateral head displacement.

those of wild-type male mice (Figures 6C and 6D). Additionally, three kinematic parameters, including curvilinear velocity (VCL), straight-line velocity (VSL), and average-path velocity (VAP), were significantly lower in *Cfap47*-mutated male mice than in wild-type male mice (Figure 6E). Regarding sperm concentration, there was no obvious difference between wild-type and *Cfap47*-mutated male mice (Table S6). H&E staining and SEM assay revealed that bent flagella were frequently observed in *Cfap47*-mutated male mice (Figure 7). Remarkably, the bent flagella most likely appeared first in the corpus of epididymis, but not in the testis of *Cfap47*-mutated male mice (Videos S3–S8 and Figure S12). Furthermore, although no obvious abnormal ultrastructure was detected in cross sections of the spermatozoa from *Cfap47*-mutated male mice, a higher rate of unevenly distributed fibrous sheaths was observed in the spermatozoa from *Cfap47*-mutated male mice than in those from wild-type male mice (Figures S13 and S14). These experimental observations suggested the possibility of abnormal sperm maturation in the epididymis of *Cfap47*-mutated male mice and/or sperm flagellar frangibility to mechanical stress due to the potential abnormality in flagellar assembly.

Damaged male fertility of *Cfap47*-mutated mice can be rescued by ICSI treatment

To investigate the fertility and reproductive behavior of *Cfap47*-mutated mice, we caged the sexually mature (6 weeks of age or older) wild-type and *Cfap47*-mutated male mice to age-matched wild-type females (one male with two females) for 3 months and counted the numbers of pups per litter. As shown in Figure S15, wild-type male mice routinely produced offspring (3–4 litters produced per female, 8 ± 0.82 pups per litter), whereas *Cfap47*-mutated male mice failed to produce any offspring over 3 months of breeding. We also performed IVF analysis to further investigate the fertility of *Cfap47*-mutated male mice. As expected, the rates of two-cell embryos and blastocysts were significantly lower in the group using the spermatozoa from *Cfap47*-mutated male mice than those of the wild-type male control group (Figure 8A). All these findings indicated that *Cfap47* deficiency causes male infertility in mice.

ICSI treatment has been suggested as an effective way to circumvent the physical limitations experienced by MMAF sperm.[37] To investigate whether mouse *Cfap47*-associated asthenoteratozoospermia could be overcome via ICSI, we performed ICSI by using spermatozoa from wild-type and *Cfap47*-mutated male mice. Notably, the rates of two-cell embryos and blastocysts generated by *Cfap47*-mutated male mice were comparable to those generated by wild-type male mice (Figure 8B). Similarly, three out of the four men harboring hemizygous *CFAP47* variants in this study achieved good clinical outcomes after assisted

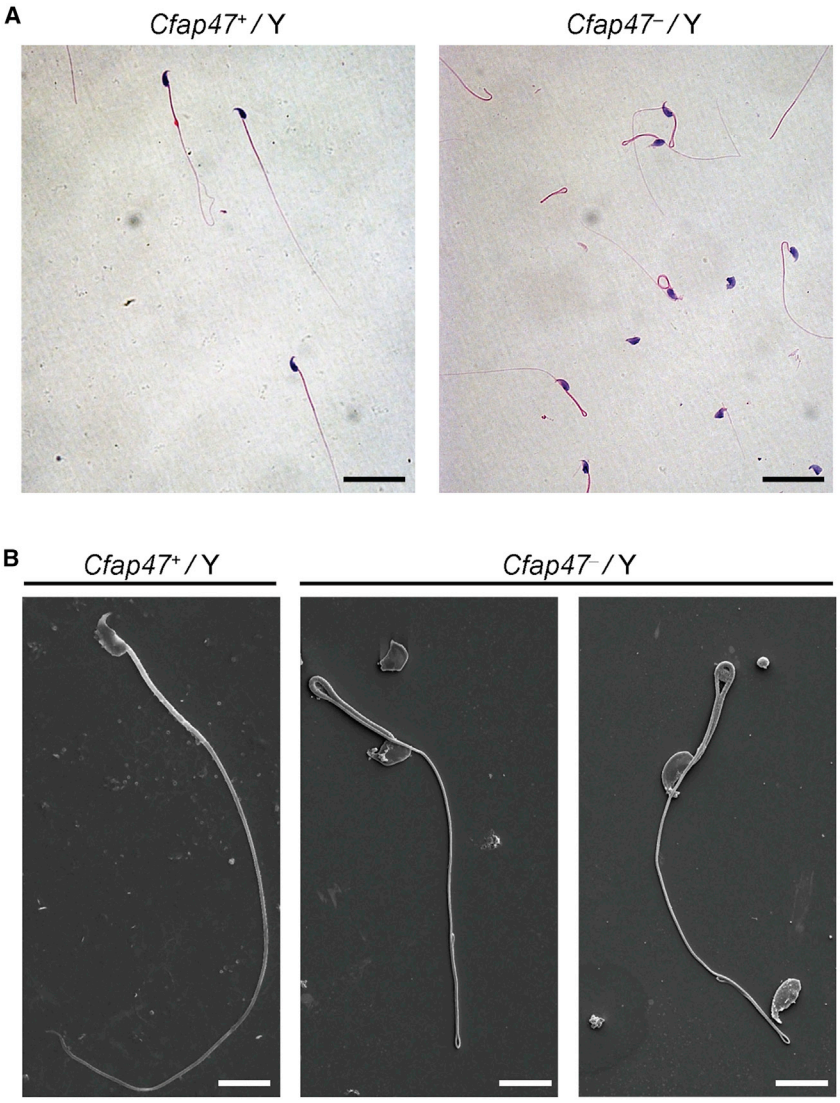

Figure 7. Sperm morphology analysis for *Cfap47*-mutated male mice

H&E staining (A) and SEM analyses (B) revealed higher rates of bent flagella in the spermatozoa of *Cfap47*-mutated (*Cfap47*$^{-}$/Y) male mice when compared with those of wild-type (*Cfap47*$^{+}$/Y) male mice. Scale bars: 20 μm (A) and 5 μm (B).

reproductive therapy by ICSI (Table 3). The fourth couple (subject T115 II-1 and his wife) could not achieve a pregnancy, potentially because of additional female risk factors of infertility (e.g., advanced reproductive age and poor oocyte quality). Therefore, our studies strongly indicated that the damaged male fertility caused by hemizygous *CFAP47* variants can be rescued by ICSI treatment.

Discussion

Since the initial identification of *DNAH1* in 2014 as a pathogenic gene in human asthenoteratozoospermia with MMAF, only an autosomal recessive inheritance has been proposed for MMAF,[4] and an additional 21 such autosomal genes have been confirmed to cause human MMAF.[4–9] Here, we demonstrated that MMAF can be caused by hemizygous mutations in an X-linked gene. We report that hemizygous deleterious variants of X-linked *CFAP47* induce severe asthenoteratozoospermia in four unrelated MMAF-affected individuals from different geographical origins. All these deleterious variants identified in *CFAP47* are absent from human population genome datasets archived in the 1000 Genomes Project, gnomAD, or DGV (Figure 1 and Table 1). Functional experiments further indicated the deficiency of CFAP47 in the spermatozoa from men harboring hemizygous *CFAP47* variants. All these findings indicate that *CFAP47* is an X-linked MMAF-associated gene. Analogously, the X-linked *AKAP4* (MIM: 300185) was previously found to be deleted together with an *AKAP3* deletion on the human chromosome 12 in a man with sperm fibrous sheath dysplasia, but no further molecular evidence of the transcripts or proteins was available to confirm the pathogenicity of *AKAP3* deletion and/or *AKAP4* deletion.[38] Therefore, X-linked *AKAP4* may be also a candidate gene for MMAF, but so far this has not been formally demonstrated.

To date, we do not have cues explaining the molecular mechanism by which deleterious *CFAP47* variants cause abnormal sperm morphology and/or motility. Notably, a potential interaction between CFAP65 and CFAP47 was predicted by the *in silico* tool STRING (Figure S5). Immunostaining assays performed in this study also revealed abnormal localization of CFAP65 in the spermatozoa from *CFAP47*-mutated men and the loss of CFAP47 staining in the sperm cells from *CFAP65*-mutated men. Moreover, co-immunoprecipitation assays performed on the spermatozoa from a fertile control man and the testes of wild-type male mice further support a functional link between these two cilia- and flagella-associated proteins. Previous studies also reported that *CFAP65* deficiency caused severe asthenoteratozoospermia in mice and humans.[28,31–33] Moreover, CFAP65 was found to participate in calcium-mediated retrograde signaling affecting cell differentiation and proliferation.[32,39] Thus, the reduced sperm motility and higher rates of abnormal sperm morphologies in men harboring hemizygous *CFAP47* variants may partially result from the abnormal interaction or regulation between CFAP47 and CFAP65.

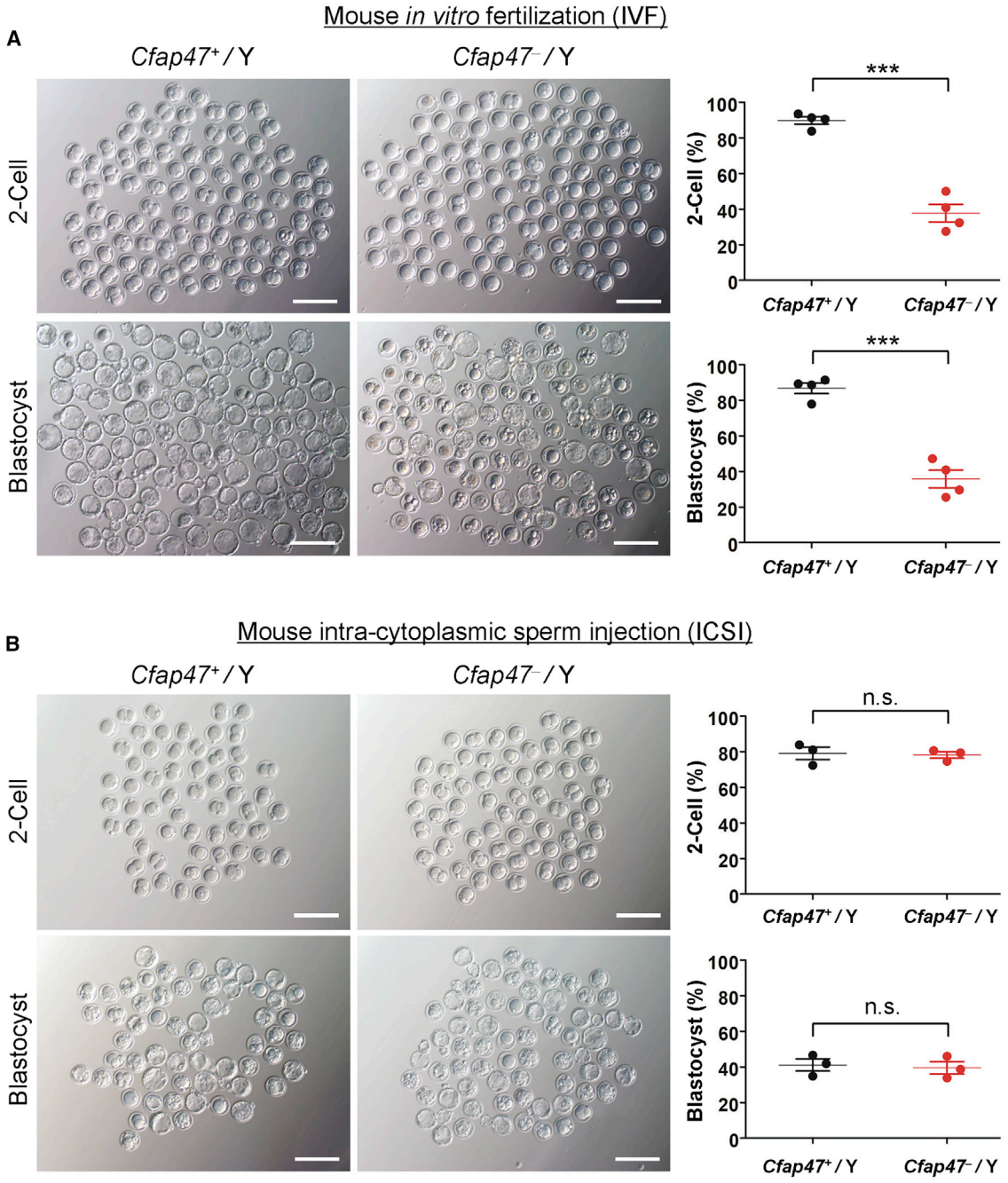

Figure 8. Damaged fertilization capability by deficiency of mouse CFAP47 could be rescued by ICSI

(A) Representative two-cell embryos and blastocysts from IVF in mice. The rates of both two-cell embryos and blastocysts were significantly lower in the group using the spermatozoa from *Cfap47*-mutated (*Cfap47*$^{-}$/Y) male mice than those in the wild-type (*Cfap47*$^{+}$/Y) group. Both groups consisted of four male mice. A total of 716 mouse embryos were counted. Data are represented as means ± standard error of measurement; ***$p < 0.001$. Scale bars: 200 μm.

(B) Representative two-cell embryos and blastocysts from ICSI in mice. The rates of two-cell embryos and blastocysts were counted after sperm heads were injected into oocytes that were collected from superovulated wild-type female mice. Both the *Cfap47*$^{+}$/Y and *Cfap47*$^{-}$/Y groups consisted of three male mice. A total of 367 mouse embryos were counted. Data are represented as means ± standard error of measurement. n.s., not significant. Scale bars: 200 μm.

We also constructed *Cfap47*-mutated mice in this study to further explore the effect of CFAP47 deficiency on sperm flagellar formation. Consistent with clinical presentation of men harboring hemizygous deleterious variants in *CFAP47*, *Cfap47*-mutated male mice were sterile and displayed reduced sperm motility. Light microscopy analysis revealed a higher rate of bent flagella in *Cfap47*-mutated male mice than in wild-type mice, a phenotype first discovered in the corpus epididymides, but not in the testis of the *Cfap47*-mutated male mice. It is well-established

Table 3. Clinical outcomes of ICSI cycles using the spermatozoa from men harboring hemizygous *CFAP47* variants

Subject	T115 II-1	T176 II-1	H025 II-1	MA2603 II-1
Male age (years)	37	26	34	31
Female age (years)	41	26	32	N/A
Number of ICSI cycles	1	1	1	1
Number of oocytes injected	1	9	11	12
Number (and rate) of fertilized oocytes	0 (0%)	8 (89%)	9 (82%)	10 (83%)
Number (and rate) of cleavage embryos	–	8 (100%)	9 (100%)	N/A
Number (and rate) of 8-cells	–	5 (63%)	7 (78%)	N/A
Number (and rate) of blastocysts	–	5 (63%)	7 (78%)	3 (30%)
Number of transfer cycles	–	1	1	3
Number of embryos transferred per cycle	–	2	2	1
Implantation rate	–	100%	50%	66%
Clinical pregnancy rate	–	100%	100%	100%
Miscarriage rate	–	0%	0%	33%

–, not applicable; N/A, not available.

that the epididymis constitutes a critical place for spermatozoa to acquire their fertilizing ability and, in particular, forward motility properties.[40] Thus, a possible impairment of sperm maturation may also occur as a result of the deficiency of mouse CFAP47. In addition, TEM assessment revealed a higher rate of unevenly distributed fibrous sheaths in the spermatozoa from *Cfap47*-mutated male mice than those from wild-type male mice, indicating potential abnormalities in flagellar assembly. It is possible that those fibrous sheath defects could confer the fragility to the sperm flagella, which may further induce bending during epididymal transit and contribute to the compromised sperm motility.[41]

Overall, the sperm phenotype of *Cfap47*-mutated male mice appears milder than the phenotype of men harboring hemizygous *CFAP47* variants. This could be due to evolutionarily divergent protein regulatory networks of CFAP47 or distinct compensatory mechanisms between species or differences in environmental exposure. Nonetheless, our investigations using CASA demonstrate significantly diminished sperm motility and abnormal sperm movements in *Cfap47*-mutated male mice. As such, the cause of sterility in *Cfap47*-mutated male mice is almost certainly due to the inability of sperm to ascend the female reproductive tract and reach the site of fertilization.

ICSI has become an effective method to help infertile couples to achieve a successful pregnancy. For infertile men with MMAF, ICSI treatment constitutes the only choice because of the constitutive flagellar defects.[42] Previous studies and our recent works revealed the good prognosis of ICSI for a series of MMAF-related genes. For example, MMAF-affected individuals with bi-allelic variants in *DNAH1*, *DNAH8*, or *TTC29* have good clinical outcomes following ICSI, while failed pregnancies were reported for *CEP135* (due to abnormal centriole assembly)- or *DNAH17* (due to unknown reason)-associated MMAF.[7,17,37,43,44] In this study, despite the reduction in fertilization observed in mouse IVF using the spermatozoa from *Cfap47*-mutated male mice, the fertilization (two-cell embryo) rate and blastocyst rate when performing ICSI for *Cfap47*-mutated male mice were similar to those observed for wild-type males. Moreover, men harboring hemizygous *CFAP47* variants in this study (except for subject T115 II-1, whose wife had poor oocyte quality) acquired successful pregnancies after ICSI treatment, further supporting that ICSI can be recommended for *CFAP47*-associated asthenoteratozoospermia.

Importantly, while both men harboring deleterious variants in X-linked *CFAP47* and those harboring bi-allelic mutations in autosomal MMAF-associated genes can have offspring via ICSI treatment, different rates of mutation carriers and different risks of male infertility in the offspring are expected between those two modes of inheritance. For the affected men whose MMAF is caused by autosomal recessive variants, both male and female offspring will be fertile heterozygous carriers who may ultimately transmit the autosomal recessive variants to next generations at a 50% probability. Assuming that there are no consanguineous conceptions, in this case of autosomal MMAF loci, the recurrence risk of MMAF will be very low for the offspring. In contrast, for ICSI performed in case of X-linked *CFAP47*-associated MMAF, 100% of female (but no male) offspring will inherit heterozygous deleterious variants of *CFAP47*. These female heterozygous carrier offspring will transmit the X-linked *CFAP47* variants at a 50% probability to the next generations, among which the females will be heterozygous carriers and the males harboring hemizygous *CFAP47* variants will be infertile. Therefore, the findings of this study are meaningful to genetic counseling for X-linked MMAF and asthenoteratozoospermia before ICSI treatment.

In conclusion, our experimental observations on both human subjects and the mouse model indicate that hemizygous *CFAP47* variants can induce MMAF-associated asthenoteratozoospermia. The observed functional associations between CFAP47 and CFAP65 indicated that cilia- and flagella-associated proteins may exist in a mutually regulated manner during spermatogenesis. Furthermore, good pregnancy outcomes could be achieved through ICSI treatment using the spermatozoa from men harboring hemizygous *CFAP47* variants. Overall, our findings provide important information for genetic counselors and clinicians to further understand the genetic causes of male infertility and establish a personalized treatment plan.

Data and code availability

The NCBI reference sequence numbers for human *CFAP47* transcript, CFAP47, and mouse *Cfap47* transcript are GenBank: NM_001304548.2, NP_001291477.1, and NM_001368718.2, respectively.

Supplemental Information

Supplemental Information can be found online at https://doi.org/10.1016/j.ajhg.2021.01.002.

Acknowledgments

We would like to thank the families for participating and supporting this study. We also thank the Center of Cryo-electron Microscopy at Zhejiang University for technical support. This work was supported by National Natural Science Foundation of China (31625015, 31521003, 81971447, 81971441, 81871216, 81901541, and 81601340), Shanghai Municipal Science and Technology Major Project (2017SHZDZX01), China Postdoctoral Science Foundation (2020TQ0072 and 2019M662786), State Key Laboratory of Reproductive Medicine (SKLRM-K202002), Science and Technology Major Project of Inner Mongolia Autonomous Region of China (zdzx2018065), the key grant of prevention and treatment of birth defect from Hunan Province (2019SK1012), the National Key Research and Developmental Program of China (2018YFC1004900), Shanghai Municipal Commission for Science and Technology (19QA1407500 and 18ZR1432300), Foundation of the Department of Science and Technology of Anhui Province (2017070802D150), the Non-profit Central Research Institute Fund of Chinese Academy of Medical Sciences (2019PT310002), the National Key Research and Development Program of China (2016YFC1000204), the Agence Nationale pour la Recherche (FLAGEL-OME ANR-19-CE17-0014), and Innovative Research Team of High-level Local Universities in Shanghai (SSMU-ZLCX20180500). The sequencing and analysis of Australian patients was supported in part by a grant from the National Health and Medical Research Council (APP1120356) and an Investigator Award in Science from The Wellcome Trust (209451). We acknowledge the ongoing support of Professor Rob McLachlan and the Monash IVF Group of infertility clinics in Australia for their role in patient recruitment and treatment.

Declaration of interests

Moira K. O'Bryan is a member of the Monash IVF Research and Education Foundation steering committee. The other authors declare no competing interests.

Received: September 30, 2020
Accepted: December 29, 2020
Published: January 19, 2021

Web resources

1000 Genomes Project, https://www.internationalgenome.org/
AnnotSV, https://lbgi.fr/AnnotSV/
CADD, https://cadd.gs.washington.edu/snv
Database of Genomic Variations, http://dgv.tcag.ca/dgv/app/home
gnomAD, https://gnomad.broadinstitute.org
HOPE, https://www3.cmbi.umcn.nl/hope/
HUGO Gene Nomenclature Committee, https://www.genenames.org/
M-CAP, http://bejerano.stanford.edu/MCAP/
National Center for Biotechnology Information (NCBI), https://www.ncbi.nlm.nih.gov/
Online Mendelian Inheritance in Man (OMIM), https://omim.org/
Picard, https://github.com/broadinstitute/picard
PolyPhen-2, http://genetics.bwh.harvard.edu/pph2/
SIFT, https://sift.bii.a-star.edu.sg
STRING, https://string-db.org/
SWISS-MODEL, https://swissmodel.expasy.org/
UCSC Genome Browser, http://genome.ucsc.edu
UCSF Chimera, http://www.cgl.ucsf.edu/chimera
UniProt, https://www.uniprot.org

References

1. Matzuk, M.M., and Lamb, D.J. (2002). Genetic dissection of mammalian fertility pathways. Nat. Cell Biol. *4* (*Suppl*), s41–s49.
2. Tournaye, H., Krausz, C., and Oates, R.D. (2017). Novel concepts in the aetiology of male reproductive impairment. Lancet Diabetes Endocrinol. *5*, 544–553.
3. Shahrokhi, S.Z., Salehi, P., Alyasin, A., Taghiyar, S., and Deemeh, M.R. (2020). Asthenozoospermia: Cellular and molecular contributing factors and treatment strategies. Andrologia *52*, e13463.
4. Ben Khelifa, M., Coutton, C., Zouari, R., Karaouzène, T., Rendu, J., Bidart, M., Yassine, S., Pierre, V., Delaroche, J., Hennebicq, S., et al. (2014). Mutations in DNAH1, which encodes an inner arm heavy chain dynein, lead to male infertility from multiple morphological abnormalities of the sperm flagella. Am. J. Hum. Genet. *94*, 95–104.
5. Touré, A., Martinez, G., Kherraf, Z.E., Cazin, C., Beurois, J., Arnoult, C., Ray, P.F., and Coutton, C. (2020). The genetic architecture of morphological abnormalities of the sperm tail. Hum. Genet. https://doi.org/10.1007/s00439-00020-02113-x.
6. Lv, M., Liu, W., Chi, W., Ni, X., Wang, J., Cheng, H., Li, W.Y., Yang, S., Wu, H., Zhang, J., et al. (2020). Homozygous mutations in *DZIP1* can induce asthenoteratospermia with severe MMAF. J. Med. Genet. *57*, 445–453.
7. Liu, C., Miyata, H., Gao, Y., Sha, Y., Tang, S., Xu, Z., Whitfield, M., Patrat, C., Wu, H., Dulioust, E., et al. (2020). Bi-allelic DNAH8 Variants Lead to Multiple Morphological Abnormalities of the Sperm Flagella and Primary Male Infertility. Am. J. Hum. Genet. *107*, 330–341.
8. Martinez, G., Beurois, J., Dacheux, D., Cazin, C., Bidart, M., Kherraf, Z.E., Robinson, D.R., Satre, V., Le Gac, G., Ka, C., et al. (2020). Biallelic variants in *MAATS1* encoding CFAP91, a calmodulin-associated and spoke-associated complex protein, cause severe astheno-teratozoospermia and male infertility. J. Med. Genet. *57*, 708–716.
9. He, X., Liu, C., Yang, X., Lv, M., Ni, X., Li, Q., Cheng, H., Liu, W., Tian, S., Wu, H., et al. (2020). Bi-allelic Loss-of-function Variants in CFAP58 Cause Flagellar Axoneme and Mitochondrial Sheath Defects and Asthenoteratozoospermia in Humans and Mice. Am. J. Hum. Genet. *107*, 514–526.

10. Skaletsky, H., Kuroda-Kawaguchi, T., Minx, P.J., Cordum, H.S., Hillier, L., Brown, L.G., Repping, S., Pyntikova, T., Ali, J., Bieri, T., et al. (2003). The male-specific region of the human Y chromosome is a mosaic of discrete sequence classes. Nature *423*, 825–837.
11. Mueller, J.L., Mahadevaiah, S.K., Park, P.J., Warburton, P.E., Page, D.C., and Turner, J.M.A. (2008). The mouse X chromosome is enriched for multicopy testis genes showing postmeiotic expression. Nat. Genet. *40*, 794–799.
12. Vockel, M., Riera-Escamilla, A., Tüttelmann, F., and Krausz, C. (2019). The X chromosome and male infertility. Hum. Genet. https://doi.org/10.1007/s00439-00019-02101-w.
13. Vogt, P.H., Edelmann, A., Kirsch, S., Henegariu, O., Hirschmann, P., Kiesewetter, F., Köhn, F.M., Schill, W.B., Farah, S., Ramos, C., et al. (1996). Human Y chromosome azoospermia factors (AZF) mapped to different subregions in Yq11. Hum. Mol. Genet. *5*, 933–943.
14. Yatsenko, A.N., Georgiadis, A.P., Röpke, A., Berman, A.J., Jaffe, T., Olszewska, M., Westernströer, B., Sanfilippo, J., Kurpisz, M., Rajkovic, A., et al. (2015). X-linked TEX11 mutations, meiotic arrest, and azoospermia in infertile men. N. Engl. J. Med. *372*, 2097–2107.
15. Patat, O., Pagin, A., Siegfried, A., Mitchell, V., Chassaing, N., Faguer, S., Monteil, L., Gaston, V., Bujan, L., Courtade-Saïdi, M., et al. (2016). Truncating Mutations in the Adhesion G Protein-Coupled Receptor G2 Gene ADGRG2 Cause an X-Linked Congenital Bilateral Absence of Vas Deferens. Am. J. Hum. Genet. *99*, 437–442.
16. Liu, W., He, X., Yang, S., Zouari, R., Wang, J., Wu, H., Kherraf, Z.E., Liu, C., Coutton, C., Zhao, R., et al. (2019). Bi-allelic Mutations in TTC21A Induce Asthenoteratospermia in Humans and Mice. Am. J. Hum. Genet. *104*, 738–748.
17. Liu, C., He, X., Liu, W., Yang, S., Wang, L., Li, W., Wu, H., Tang, S., Ni, X., Wang, J., et al. (2019). Bi-allelic Mutations in TTC29 Cause Male Subfertility with Asthenoteratospermia in Humans and Mice. Am. J. Hum. Genet. *105*, 1168–1181.
18. Li, H., and Durbin, R. (2010). Fast and accurate long-read alignment with Burrows-Wheeler transform. Bioinformatics *26*, 589–595.
19. Wang, K., Li, M., and Hakonarson, H. (2010). ANNOVAR: functional annotation of genetic variants from high-throughput sequencing data. Nucleic Acids Res. *38*, e164.
20. Ashburner, M., Ball, C.A., Blake, J.A., Botstein, D., Butler, H., Cherry, J.M., Davis, A.P., Dolinski, K., Dwight, S.S., Eppig, J.T., et al.; The Gene Ontology Consortium (2000). Gene ontology: tool for the unification of biology. Nat. Genet. *25*, 25–29.
21. Kumar, P., Henikoff, S., and Ng, P.C. (2009). Predicting the effects of coding non-synonymous variants on protein function using the SIFT algorithm. Nat. Protoc. *4*, 1073–1081.
22. Adzhubei, I.A., Schmidt, S., Peshkin, L., Ramensky, V.E., Gerasimova, A., Bork, P., Kondrashov, A.S., and Sunyaev, S.R. (2010). A method and server for predicting damaging missense mutations. Nat. Methods *7*, 248–249.
23. Schwarz, J.M., Cooper, D.N., Schuelke, M., and Seelow, D. (2014). MutationTaster2: mutation prediction for the deep-sequencing age. Nat. Methods *11*, 361–362.
24. Venselaar, H., Te Beek, T.A., Kuipers, R.K., Hekkelman, M.L., and Vriend, G. (2010). Protein structure analysis of mutations causing inheritable diseases. An e-Science approach with life scientist friendly interfaces. BMC Bioinformatics *11*, 548.
25. McKenna, A., Hanna, M., Banks, E., Sivachenko, A., Cibulskis, K., Kernytsky, A., Garimella, K., Altshuler, D., Gabriel, S., Daly, M., and DePristo, M.A. (2010). The Genome Analysis Toolkit: a MapReduce framework for analyzing next-generation DNA sequencing data. Genome Res. *20*, 1297–1303.
26. The R Development Core Team (2011). R: A Language and Environment for Statistical Computing (R Foundation for Statistical Computing).
27. Geoffroy, V., Herenger, Y., Kress, A., Stoetzel, C., Piton, A., Dollfus, H., and Muller, J. (2018). AnnotSV: an integrated tool for structural variations annotation. Bioinformatics *34*, 3572–3574.
28. Tang, S., Wang, X., Li, W., Yang, X., Li, Z., Liu, W., Li, C., Zhu, Z., Wang, L., Wang, J., et al. (2017). Biallelic Mutations in CFAP43 and CFAP44 Cause Male Infertility with Multiple Morphological Abnormalities of the Sperm Flagella. Am. J. Hum. Genet. *100*, 854–864.
29. Wang, L., Li, M.Y., Qu, C., Miao, W.Y., Yin, Q., Liao, J., Cao, H.T., Huang, M., Wang, K., Zuo, E., et al. (2017). CRISPR-Cas9-mediated genome editing in one blastomere of two-cell embryos reveals a novel Tet3 function in regulating neocortical development. Cell Res. *27*, 815–829.
30. Gu, T.P., Guo, F., Yang, H., Wu, H.P., Xu, G.F., Liu, W., Xie, Z.G., Shi, L., He, X., Jin, S.G., et al. (2011). The role of Tet3 DNA dioxygenase in epigenetic reprogramming by oocytes. Nature *477*, 606–610.
31. Li, W., Wu, H., Li, F., Tian, S., Kherraf, Z.E., Zhang, J., Ni, X., Lv, M., Liu, C., Tan, Q., et al. (2020). Biallelic mutations in *CFAP65* cause male infertility with multiple morphological abnormalities of the sperm flagella in humans and mice. J. Med. Genet. *57*, 89–95.
32. Wang, W., Tu, C., Nie, H., Meng, L., Li, Y., Yuan, S., Zhang, Q., Du, J., Wang, J., Gong, F., et al. (2019). Biallelic mutations in *CFAP65* lead to severe asthenoteratospermia due to acrosome hypoplasia and flagellum malformations. J. Med. Genet. *56*, 750–757.
33. Zhang, X., Shen, Y., Wang, X., Yuan, G., Zhang, C., and Yang, Y. (2019). A novel homozygous CFAP65 mutation in humans causes male infertility with multiple morphological abnormalities of the sperm flagella. Clin. Genet. *96*, 541–548.
34. Wang, Y., Yang, J., Jia, Y., Xiong, C., Meng, T., Guan, H., Xia, W., Ding, M., and Yuchi, M. (2014). Variability in the morphologic assessment of human sperm: use of the strict criteria recommended by the World Health Organization in 2010. Fertil. Steril. *101*, 945–949.
35. Cooper, T.G., Noonan, E., von Eckardstein, S., Auger, J., Baker, H.W., Behre, H.M., Haugen, T.B., Kruger, T., Wang, C., Mbizvo, M.T., and Vogelsong, K.M. (2010). World Health Organization reference values for human semen characteristics. Hum. Reprod. Update *16*, 231–245.
36. Auger, J., Jouannet, P., and Eustache, F. (2016). Another look at human sperm morphology. Hum. Reprod. *31*, 10–23.
37. Wambergue, C., Zouari, R., Fourati Ben Mustapha, S., Martinez, G., Devillard, F., Hennebicq, S., Satre, V., Brouillet, S., Halouani, L., Marrakchi, O., et al. (2016). Patients with multiple morphological abnormalities of the sperm flagella due to DNAH1 mutations have a good prognosis following intracytoplasmic sperm injection. Hum. Reprod. *31*, 1164–1172.

38. Baccetti, B., Collodel, G., Estenoz, M., Manca, D., Moretti, E., and Piomboni, P. (2005). Gene deletions in an infertile man with sperm fibrous sheath dysplasia. Hum. Reprod. *20*, 2790–2794.
39. Lee, W.R., Na, H., Lee, S.W., Lim, W.J., Kim, N., Lee, J.E., and Kang, C. (2017). Transcriptomic analysis of mitochondrial TFAM depletion changing cell morphology and proliferation. Sci. Rep. *7*, 17841.
40. Sullivan, R., and Mieusset, R. (2016). The human epididymis: its function in sperm maturation. Hum. Reprod. Update *22*, 574–587.
41. Eddy, E.M., Toshimori, K., and O'Brien, D.A. (2003). Fibrous sheath of mammalian spermatozoa. Microsc. Res. Tech. *61*, 103–115.
42. Chemes, H.E., and Alvarez Sedo, C. (2012). Tales of the tail and sperm head aches: changing concepts on the prognostic significance of sperm pathologies affecting the head, neck and tail. Asian J. Androl. *14*, 14–23.
43. Whitfield, M., Thomas, L., Bequignon, E., Schmitt, A., Stouvenel, L., Montantin, G., Tissier, S., Duquesnoy, P., Copin, B., Chantot, S., et al. (2019). Mutations in DNAH17, Encoding a Sperm-Specific Axonemal Outer Dynein Arm Heavy Chain, Cause Isolated Male Infertility Due to Asthenozoospermia. Am. J. Hum. Genet. *105*, 198–212.
44. Sha, Y.W., Xu, X., Mei, L.B., Li, P., Su, Z.Y., He, X.Q., and Li, L. (2017). A homozygous CEP135 mutation is associated with multiple morphological abnormalities of the sperm flagella (MMAF). Gene *633*, 48–53.

The American Journal of Human Genetics, Volume *108*

Supplemental Data

Deleterious variants in X-linked *CFAP47* induce asthenoteratozoospermia and primary male infertility

Chunyu Liu, Chaofeng Tu, Lingbo Wang, Huan Wu, Brendan J. Houston, Francesco K. Mastrorosa, Wen Zhang, Ying Shen, Jiaxiong Wang, Shixiong Tian, Lanlan Meng, Jiangshan Cong, Shenmin Yang, Yiwen Jiang, Shuyan Tang, Yuyan Zeng, Mingrong Lv, Ge Lin, Jinsong Li, Hexige Saiyin, Xiaojin He, Li Jin, Aminata Touré, Pierre F. Ray, Joris A. Veltman, Qinghua Shi, Moira K. O'Bryan, Yunxia Cao, Yue-Qiu Tan, and Feng Zhang

Supplemental Note: Case Reports

All of these male individuals displayed typical MMAF phenotypes (a combination of sperm flagellar defects, including absent, short, bent, coiled, and/or irregular-caliber flagella) with no obvious primary ciliary dyskinesia related symptoms such as sinusitis, bronchitis, pneumonia and otitis media.[1] Moreover, clinical investigations indicated that the development of male external genitalia, bilateral testicular sizes, hormone levels, and secondary sexual characteristics were normal in all of the MMAF-affected men in this study. Men with abnormalities in chromosomal karyotypes or microdeletions on the Y chromosome were also excluded. The study regarding the cohorts was approved by the institutional review boards at all the participating institutes, and signed informed consents were obtained from all subjects participating in the study.

Supplemental References

1. Knowles, M.R., Zariwala, M., and Leigh, M. (2016). Primary Ciliary Dyskinesia. Clin. Chest Med. *37*, 449-461.

M4 = GRCh37/hg19 Xp21.1(chrX:34147944-37312950) x 0

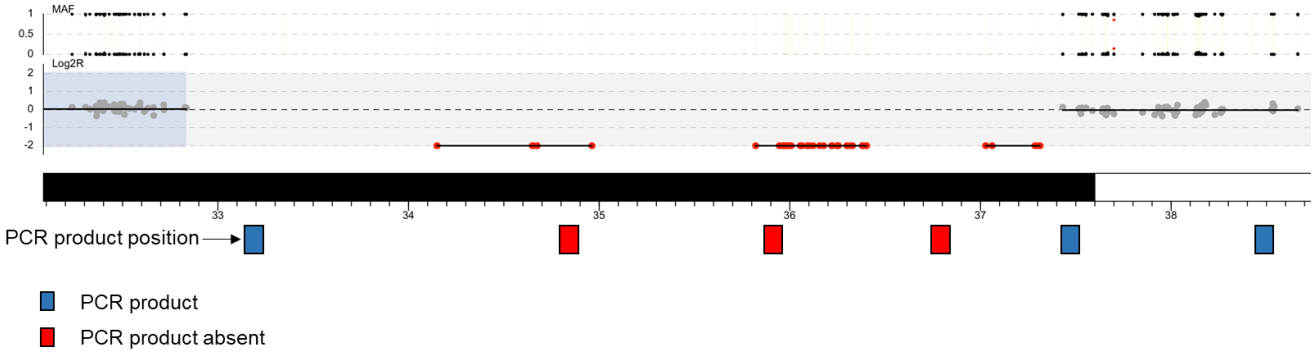

Figure S1. Verification of the Hemizygous Xp21.1 Deletion Affecting *CFAP47* using PCR Assays.

Three primer-pairs were designed to amplify the region encompassed by the deletion, while other three primer-pairs were designed to amplify the flanking regions.

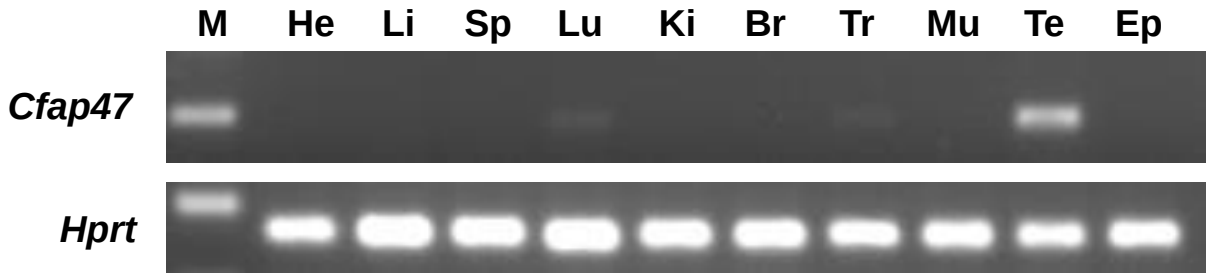

Figure S2. Gene Expressions of Mouse *Cfap47* in Different Tissues.

Expressions of *Cfap47* were investigated by RT-PCR in various tissues from adult male mice. *Hprt* was used as an internal control locus.

Abbreviations: M, marker; He, heart; Li, liver; Sp, spleen; Lu, lung; Ki, kidney; Br, brain; Tr, trachea; Mu, muscle; Te, testis; Ep, epididymis.

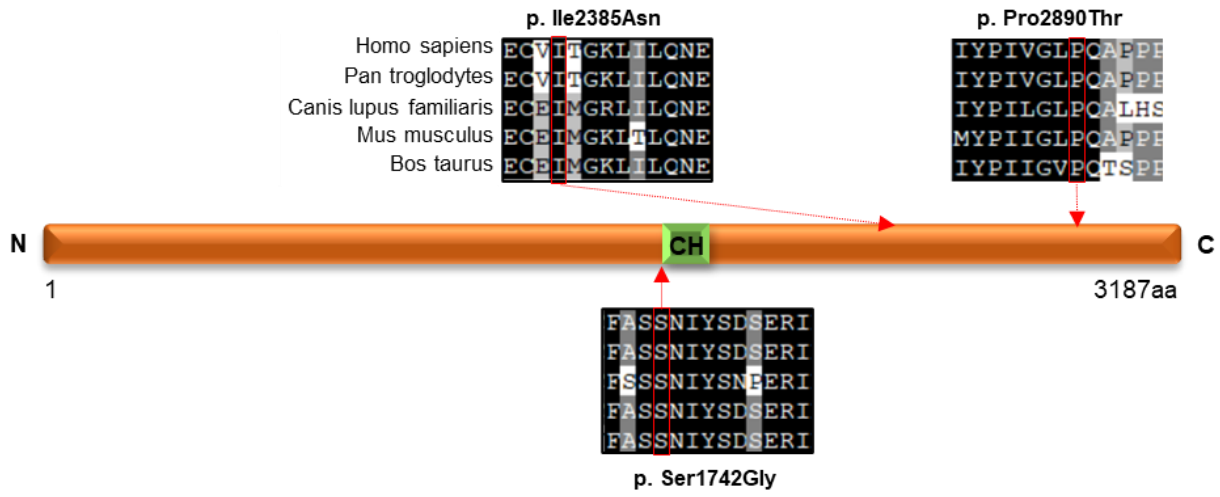

Figure S3. Phylogenetic Conservation of the Mutated Residues in CFAP47 Protein.
The CFAP47 protein contains the CH (calponin homology) domain according to the NCBI browser. The mutated residues are indicated by red boxes. The conservativeness analysis was conducted using the ClustalX2 tool. Conserved residues are marked in black (100% conservativeness), dark gray (80% conservativeness), and light gray (60% conservativeness). No shading denotes residues with less than 60% conservativeness.

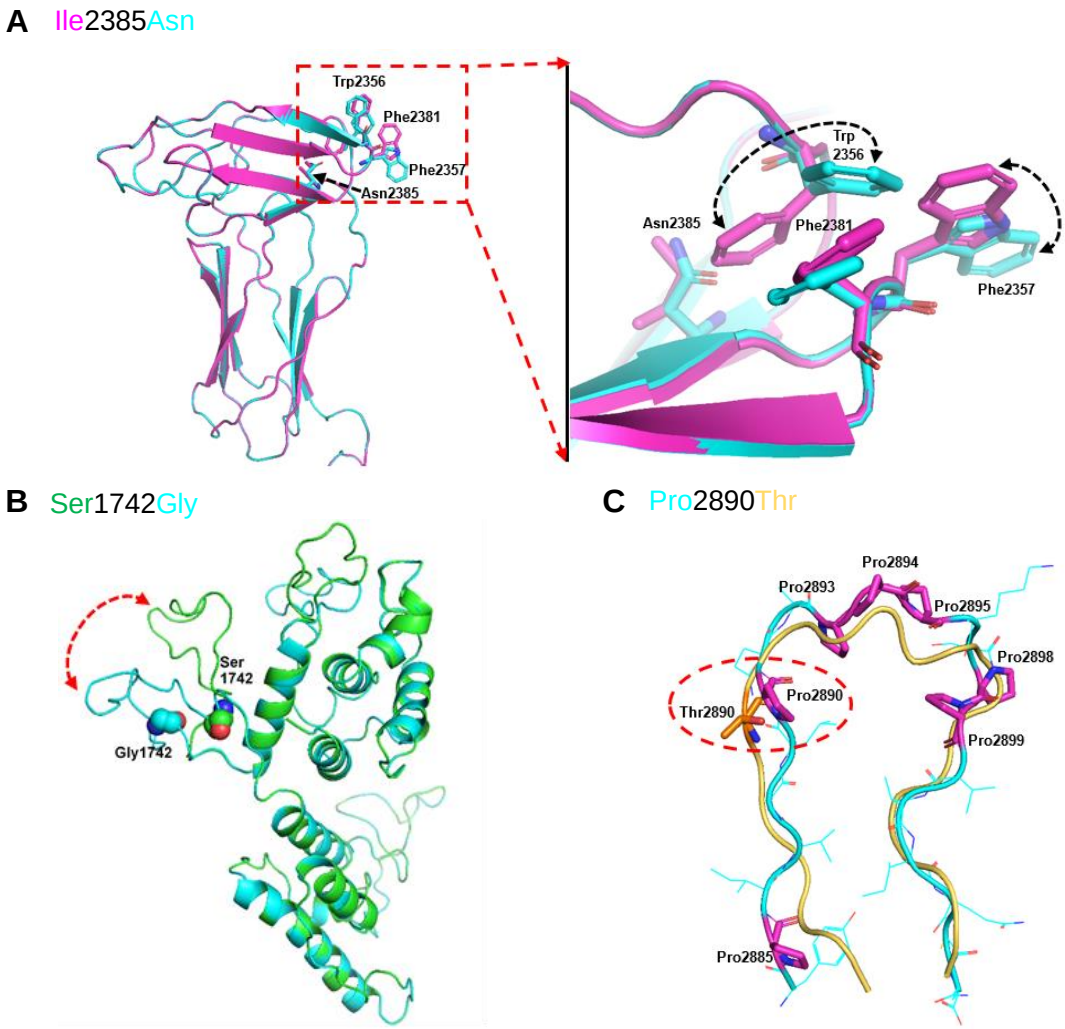

Figure S4. Effects of *CFAP47* Missense Mutations on the Structure of CFAP47 Protein.

(A) Structure model of wild-type CFAP47 protein (in pink) and the mutant p.Ile2385Asn (in blue). The mutagenesis of Ile2385Asn introduces the polar interactions and decreases the hydrophobic interactions, which may induce the nearby aromatic residue Trp2356 flipping out and exposing to surface. The corresponding movement of the surrounding aromatic residues Phe2357 and Phe2381 may increase the surface hydrophobic patch for molecular interactions as well as decrease the stability of beta sheets packing structure.

(B) Structure model of wild-type CFAP47 protein (in green) and the mutant p.Ser1742Gly (in blue). The mutagenesis of Ser1742Gly may increase the structure flexibility of backbone and loss the polar interactions, which may induce the possible local conformation change of coli-coli structure.

(C) Structure model of wild-type CFAP47 protein (in blue) and the mutant p.Pro2890Thr (in yellow). The mutagenesis of Pro2890Thr may alter the backbone flexibility, residue charge and hydrophobicity, which may decrease the stability of the loop and change the possible molecular interactions.

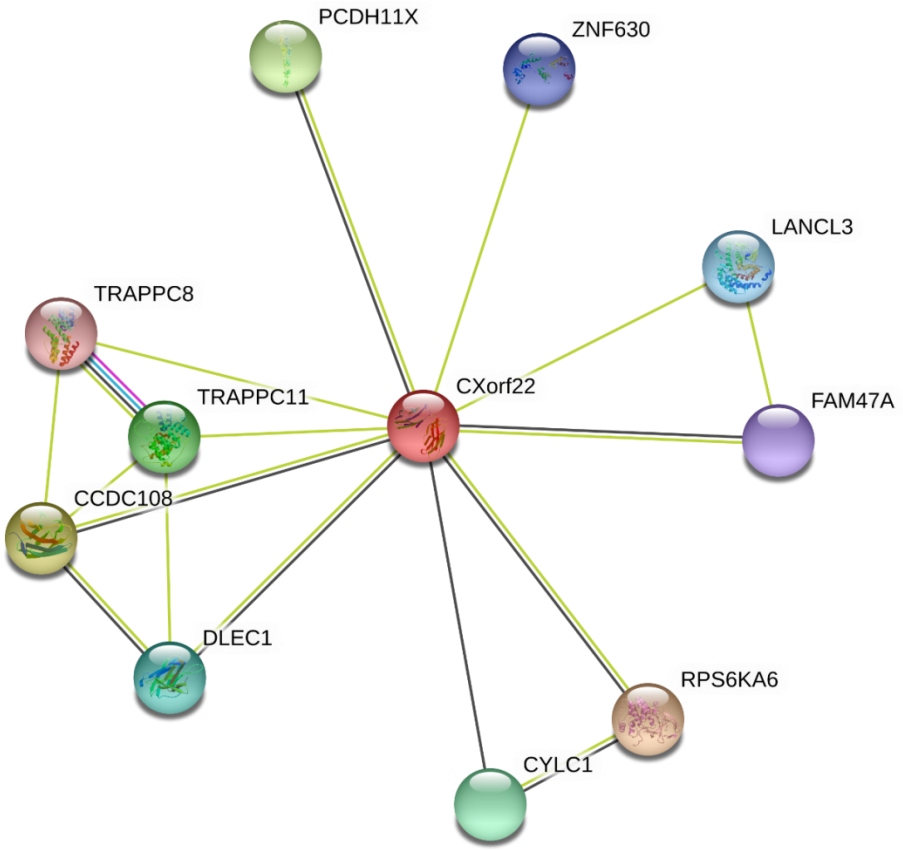

Figure S5. Protein-Protein Interaction Network for CFAP47 (CXorf22) Predicted by STRING. The protein interaction network was predicted by *in silico* software String for human CFAP47 (also known as CXorf22 in the figure) protein. A potential interaction was predicted between human CFAP47 and CFAP65 (also known as CCDC108 in the figure). Yellow lines and black lines suggest the predictions from text mining and co-expression, while pink lines and blue lines indicate the known interactions from experimental verification and curated databases.

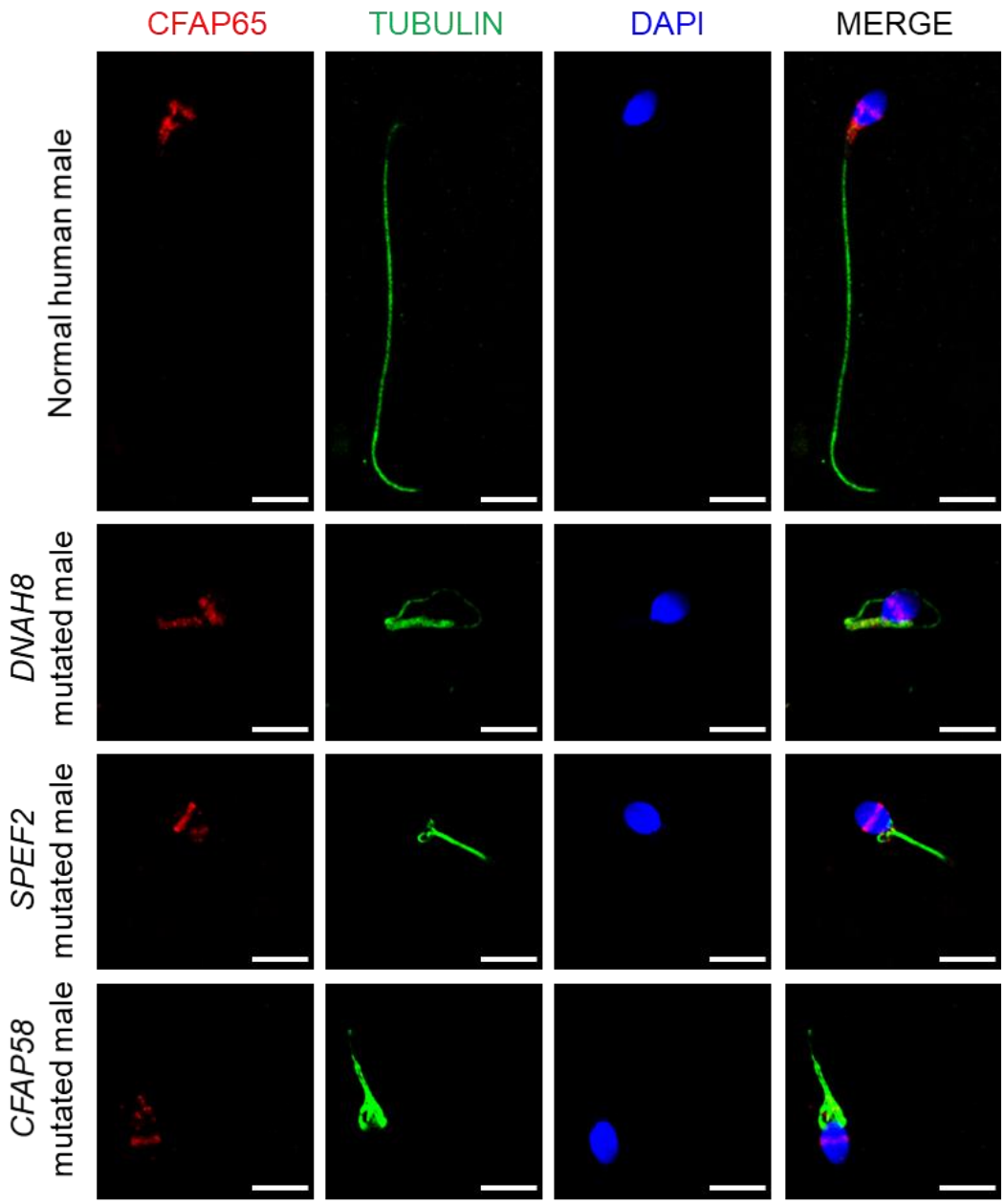

Figure S6. Immunofluorescence Staining of CFAP65 in the Spermatozoa from a Normal Male Control and MMAF-Affected Men Harboring Bi-allelic Variants in *DNAH8*, *SPEF2* or *CFAP58*.

Sperm cells were stained with anti-CFAP65 (red) and anti-α-tubulin (green) antibodies. DNA was counterstained with DAPI (4',6-diamidino-2-phenylindole) as a marker of the cell nucleus. CFAP65 staining is concentrated at the equatorial segment of sperm head and the base of flagella from both the control male and men harboring bi-allelic variants of *DNAH8*, *SPEF2* or *CFAP58*.

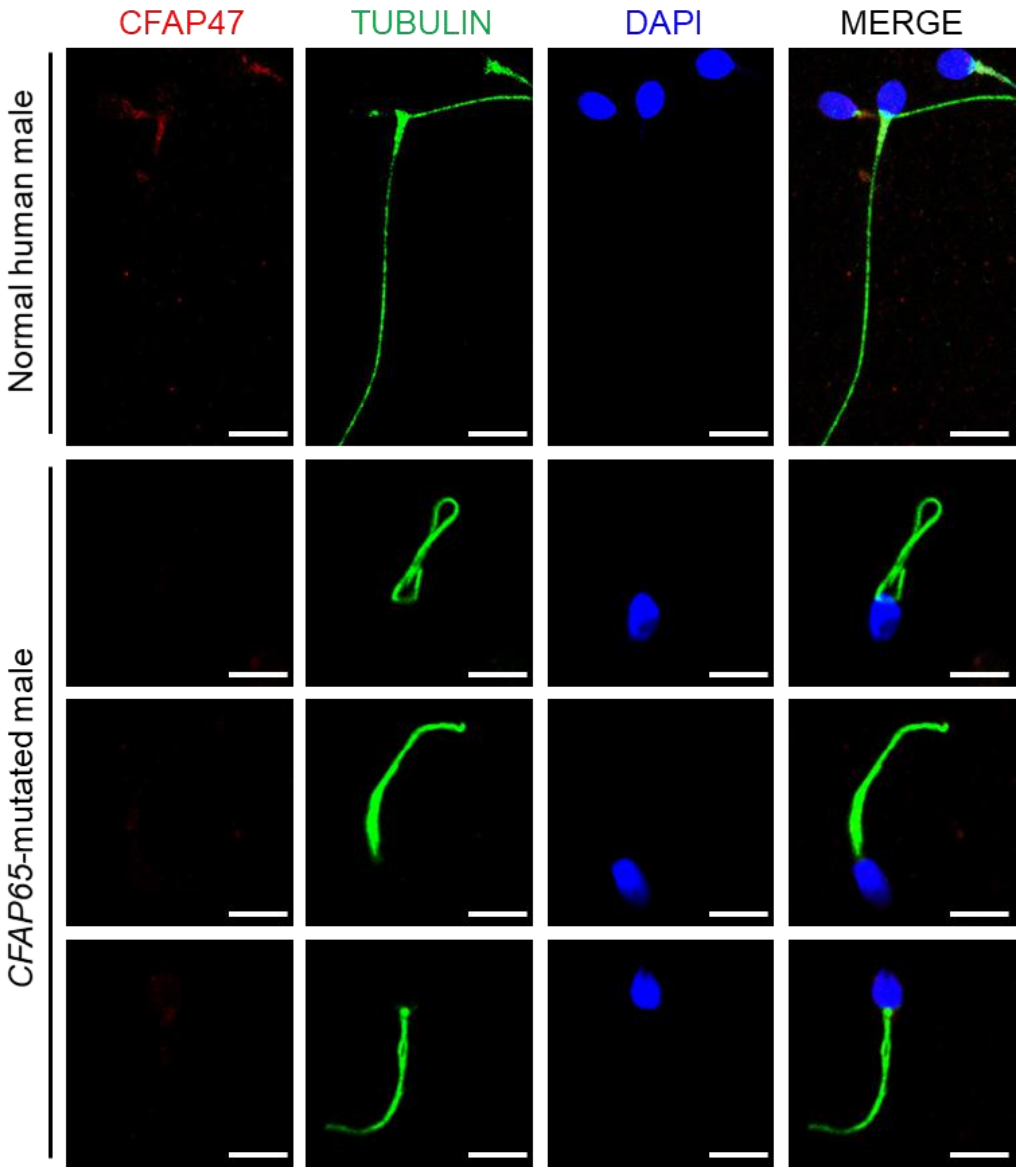

Figure S7. Reduced CFAP47 Immunostaining in the Spermatozoa from Men Harboring Bi-allelic *CFAP65* Variants.

Sperm cells were stained with anti-CFAP47 (red) and anti-α-tubulin (green) antibodies. DNA was counterstained with DAPI as a marker of the cell nucleus. In the spermatozoa from a fertile control man, CFAP47 staining appears to be located mainly in the basal body of sperm flagella. In the sperm cells from men harboring bi-allelic *CFAP65* variants, CFAP47 staining is strongly reduced or totally absent. Scale bars: 5 µm.

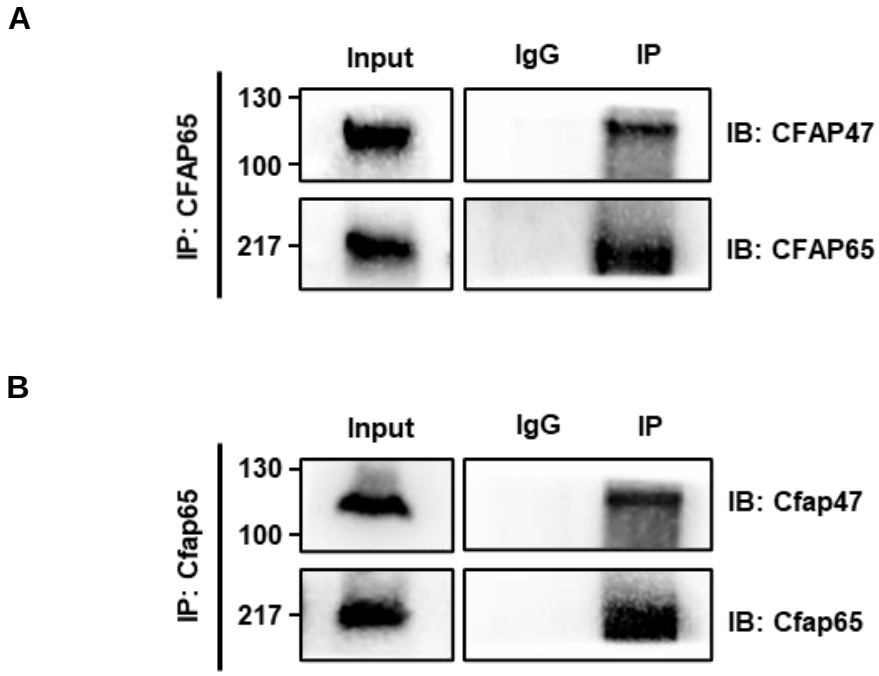

Figure S8. Co-Immunoprecipitation (Co-IP) Assays Using CFAP47/Cfap47 Antibodies Showed Interactions Between CFAP47/Cfap47 and CFAP65/Cfap65.

(A) The association between CFAP47 and CFAP65 proteins was shown in the spermatozoa from a normal control man.

(B) The association between Cfap47 and Cfap65 was shown in the testes from wild-type male mice. Input proteins and normal IgG pulldowns were used as positive and negative controls, respectively.

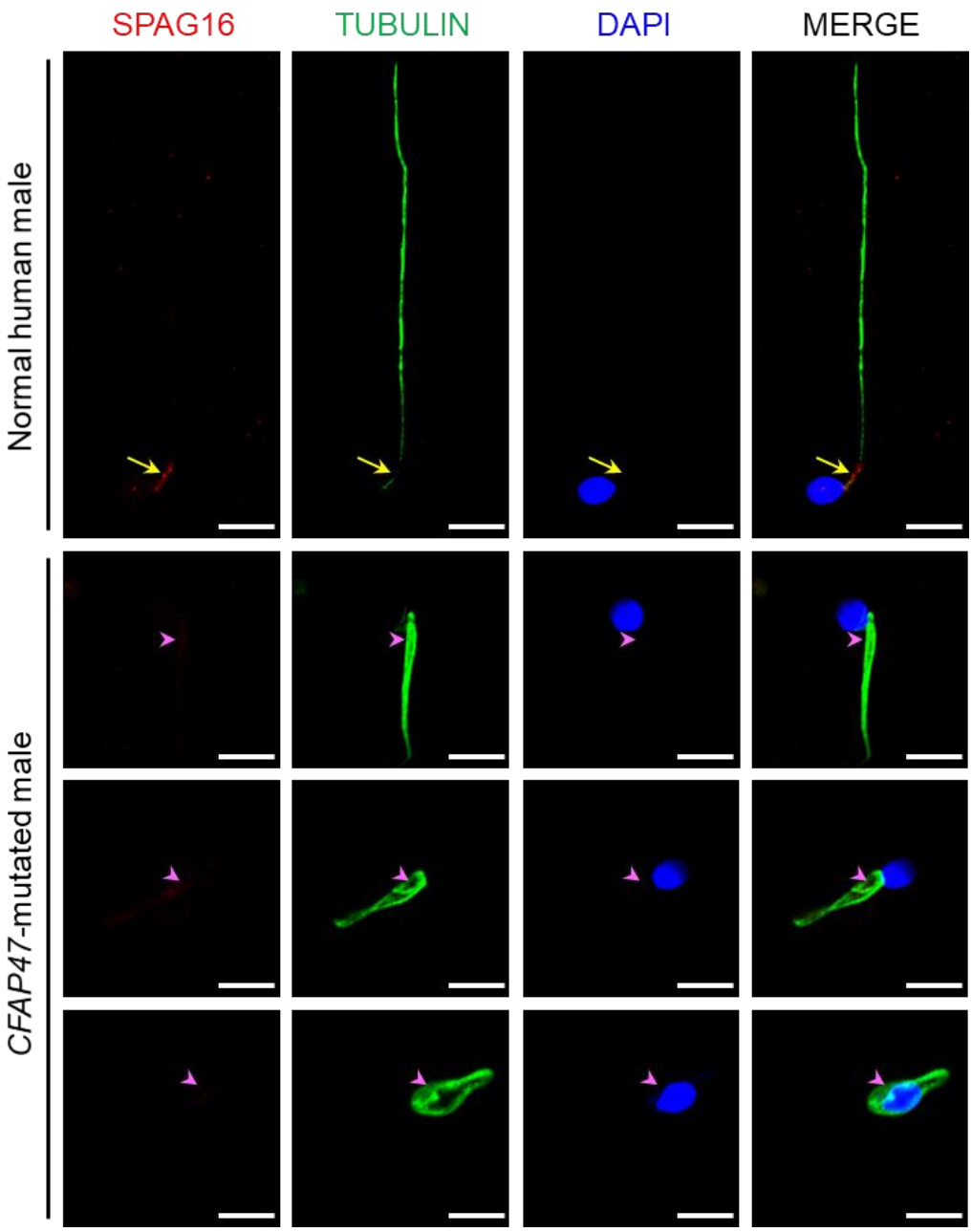

Figure S9. Immunofluorescence Staining of SPAG16 in the Spermatozoa from a Fertile Male Control and Men Harboring Hemizygous *CFAP47* Variants.

Sperm cells were stained with anti-SPAG16 (red) and anti-α-tubulin (green) antibodies. DNA was counterstained with DAPI as a marker of the cell nucleus. SPAG16 staining is concentrated at the basal body (as indicated by yellow arrows) of sperm flagella from the normal control, but the signal was almost absent (as indicated by pink arrowheads) in the sperm flagella from men harboring hemizygous *CFAP47* variants. Scale bars: 5 μm.

A

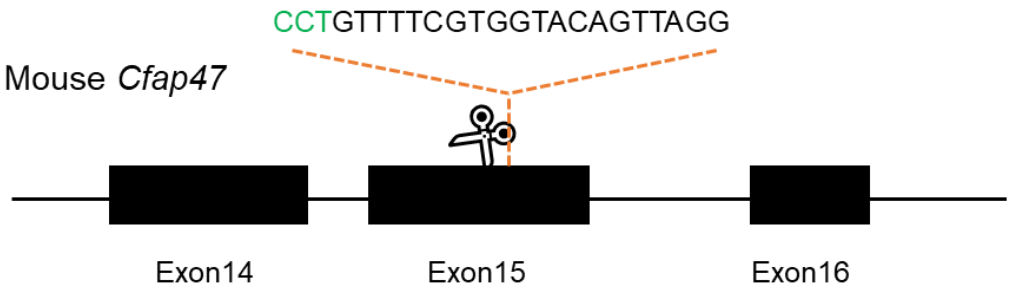

B

Figure S10. Schematic Illustration of the Targeting Strategy for Generating *Cfap47*-Mutated Mice.

(A) The gRNA was targeted in exon 15 of mouse *Cfap47*. The protospacer adjacent motif (PAM) is shown in green.

(B) A frameshift mutation (c.2559insT) was generated in mouse *Cfap47* using CRSIPR-Cas9 technology. The inserted nucleotide was predicted to cause premature translational termination (p.Gly855Profs*8) of mouse *Cfap47*. The termination codon (purple asterisk) was shown in the mutated cDNA. Abbreviation: WT, wild-type.

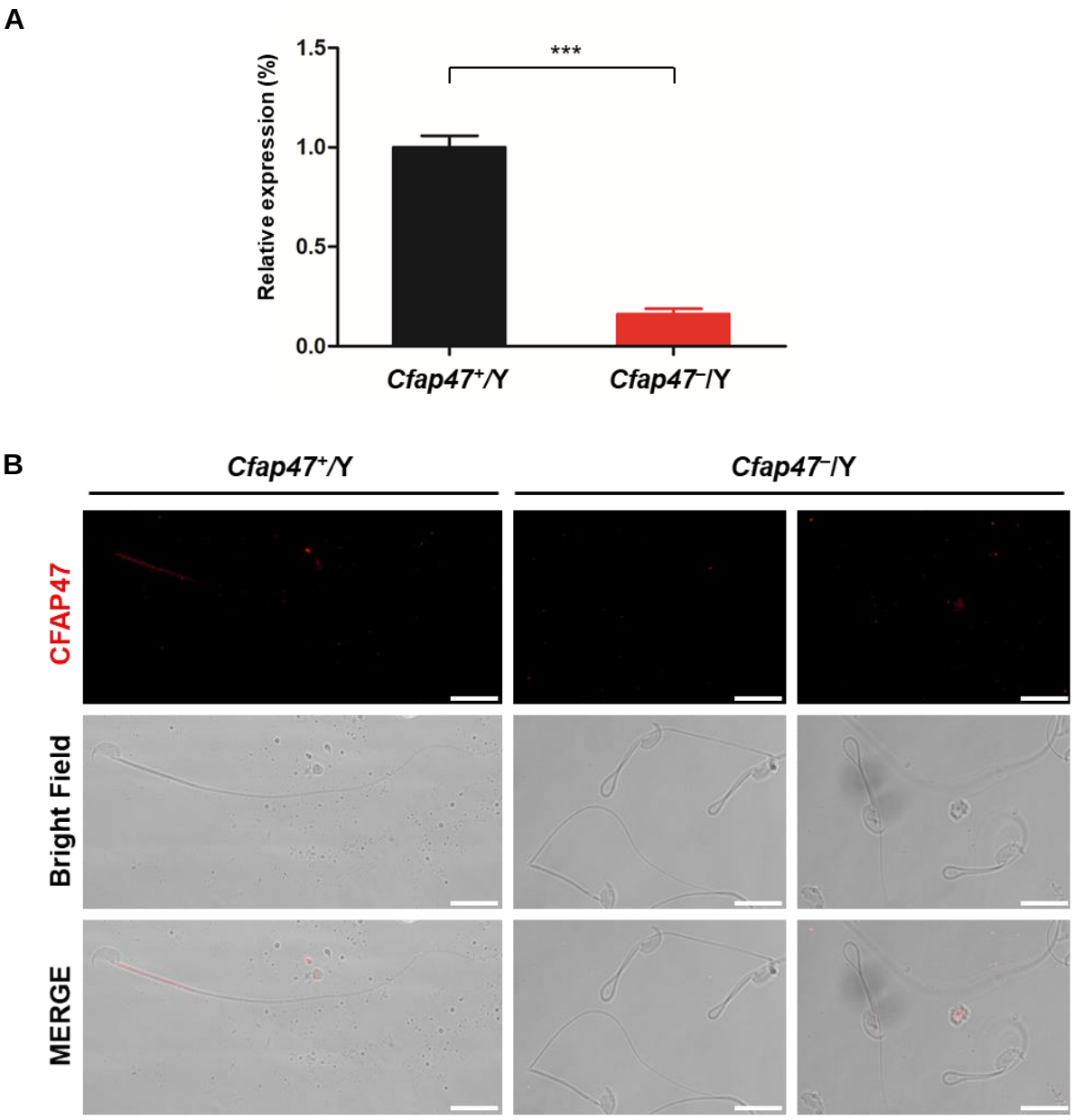

Figure S11. Expression of *Cfap47* mRNA and Location of CFAP47 Protein in the Spermatozoa from Wild-Type (*Cfap47*$^{+}$/Y) and *Cfap47*-Mutated (*Cfap47*$^{-}$/Y) Male Mice.

(A) RT-qPCR assay suggested that the level of *Cfap47* mRNA was significantly lower in the spermatozoa from *Cfap47*$^{-}$/Y male mice than that of wild-type male mice. Data represent the means ± SEM of three independent experiments. Two-tailed Student's paired or unpaired *t* tests were used as appropriate (*** $P < 0.001$).

(B) CFAP47 immunostaining showed that the CFAP47 staining (red) is concentrated in the mid-piece of the sperm flagella from wild-type male mice, but the CFAP47 signal is almost absent in the sperm flagella from *Cfap47*$^{-}$/Y male mice. Scale bars: 10 μm.

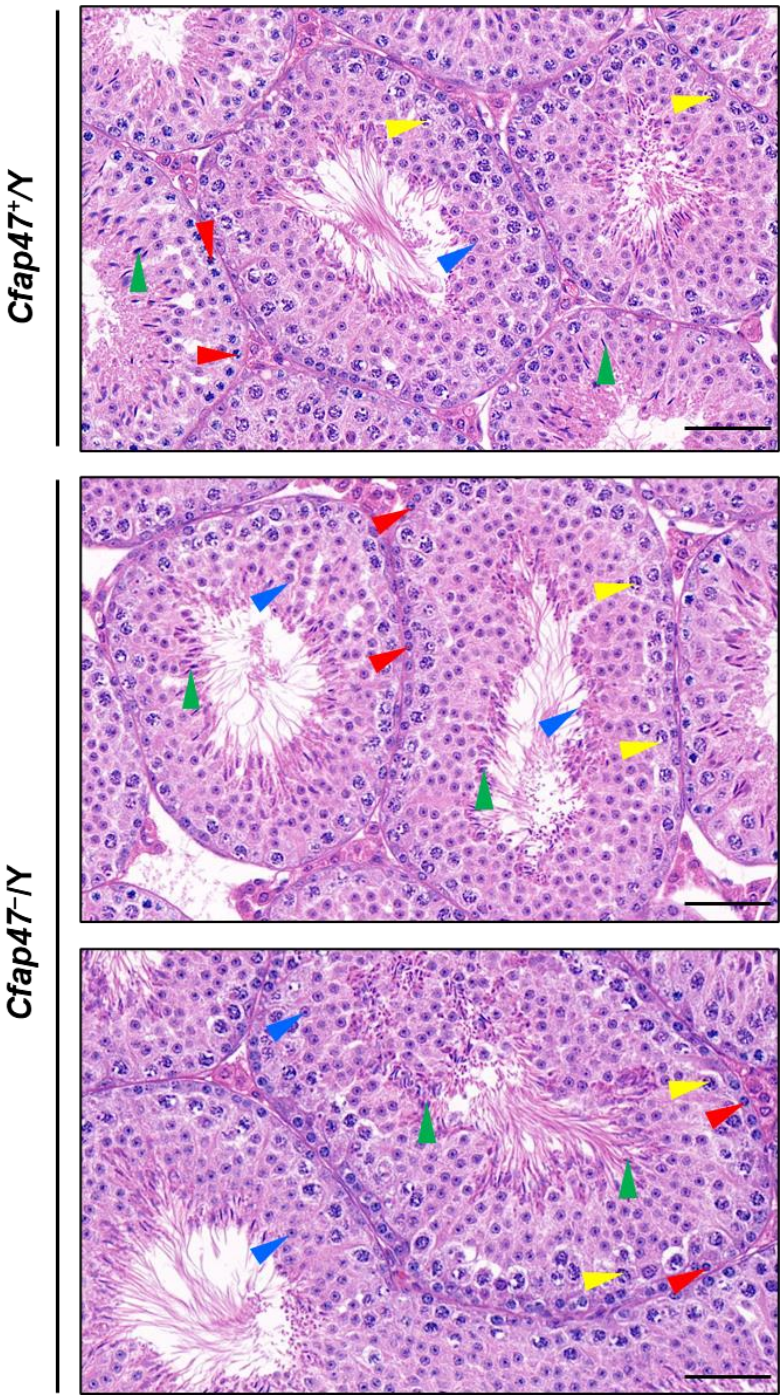

Figure S12. H&E staining of the Testicular Tissue Sections Obtained from Wild-Type (*Cfap47*$^{+}$/Y) and *Cfap47*-Mutated (*Cfap47*$^{-}$/Y) Male Mice.

H&E staining of testicular tissues showed no inter-group difference in the overall morphology of germ cells. A variety of cell types can be seen in the testes from both wild-type and *Cfap47*$^{-}$/Y male mice, including spermatogonia (red arrowheads), spermatocytes (yellow arrowheads), round spermatids (blue arrowheads) and spermatozoa (green arrowheads). Scale bars: 50 μm.

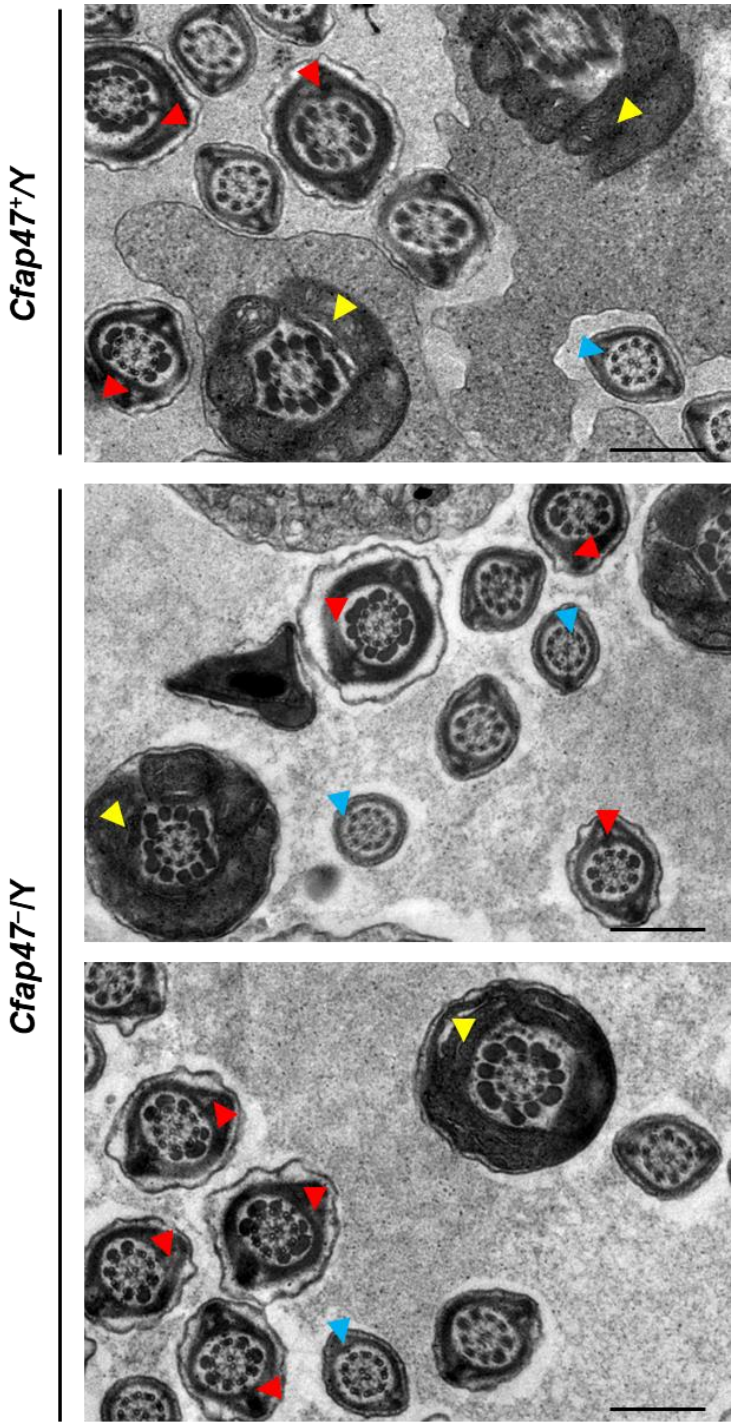

Figure S13. TEM Cross-Sections of the Spermatozoa from *Cfap47*-Mutated (*Cfap47*$^{-}$/Y) Male Mice Revealed Normal Ultrastructures.

Yellow arrowheads indicate the mid-piece, red arrowheads indicate the principal piece, and blue arrowheads indicate the end piece of sperm flagella. Scale bars: 200 nm.

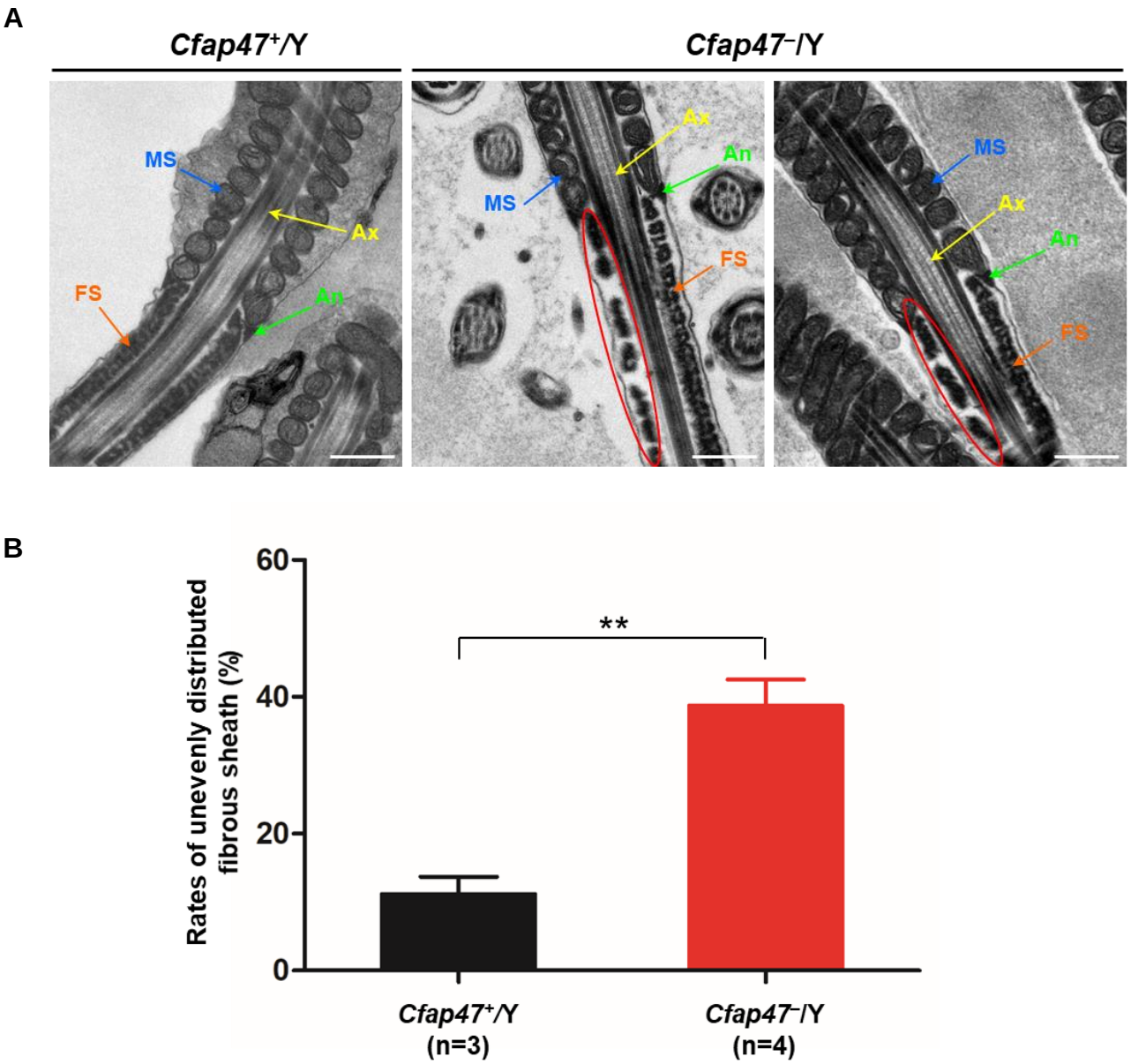

Figure S14. TEM Vertical Sections of the Spermatozoa from Wild-Type (*Cfap47*$^{+}$/Y) and *Cfap47*-Mutated (*Cfap47*$^{-}$/Y) Male Mice.

(A) Unevenly distributed fibrous sheathes (as indicated by red circles) were frequently observed in the spermatozoa from *Cfap47*$^{-}$/Y male mice. FS, fibrous sheath (orange arrows); MS, mitochondrial sheath (blue arrows); An, annulus (green arrows); Ax, axoneme (yellow arrows). Scale bars: 0.5 μm.

(B) Rates of unevenly distributed fibrous sheathes at the principal pieces of sperm flagella from *Cfap47*$^{+}$/Y and *Cfap47*$^{-}$/Y male mice. A higher rate of unevenly distributed fibrous sheathes was found in the spermatozoa from *Cfap47*$^{-}$/Y male mice than those in *Cfap47*$^{+}$/Y male mice. At least 50 sections were counted for each mouse. Data are presented as mean ± SEM (**$P < 0.01$). n, the number of male mice analyzed in this assay.

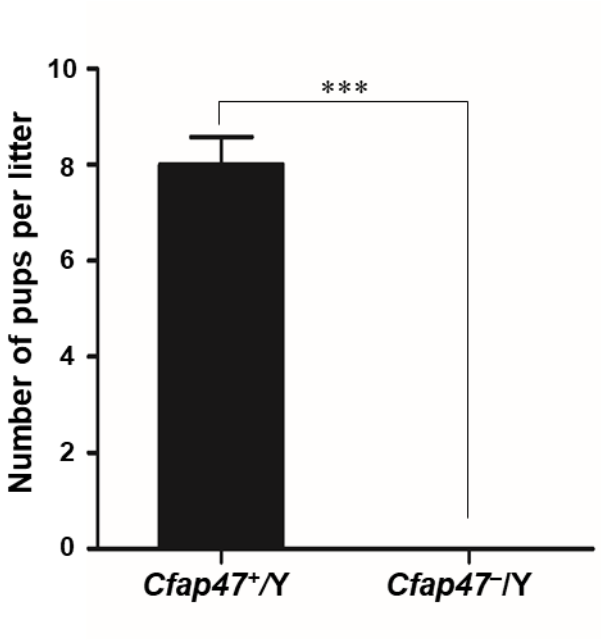

Figure S15. Fertility of Wild-Type (*Cfap47*$^{+}$/Y) and *Cfap47*-Mutated Male Mice (*Cfap47*$^{-}$/Y). Wild-type and *Cfap47*$^{-}$/Y male mice were bred with wild-type female mice, and the numbers of pups per litter were counted. Wild-type male mice routinely produced offspring, but *Cfap47*$^{-}$/Y males were sterile. (Unpaired *t* test; ***$P < 0.001$; the error bar represents S.D.)

Table S1. Primers Used for Amplification and Verification of *CFAP47* Mutations

Primer Names	Primer Sequences (5'-3')	Tm
M1-F	ACAAACGATAAATGGACCTTTCAA	58 ℃
M1-R	TGTTATGTTCATGATGTTTATGCCT	
M2-F	TAGTGCCCTCTTTAATCTCCTGT	59 ℃
M2-R	GAAAGTAAATGTTGGAGAGGGGTC	
M3-F	GCTTTGTGATGATTTTCCAGGGTTT	57 ℃
M3-R	ACATTCTGACTGGTTTGG	

Table S2. Primers Used for the Verification of the Xp21.1 Deletion Affecting *CFAP47*

PCR product ranges (hg19)	Primer Sequences (5'-3')
chrX:33147773-33147947	F: GCGGAAATTTCATTTGGAGA
	R: TAGGCAACCTCCATTTCCAT
chrX:34912831-34913051	F: CTTTGGTCCCTTTTCATGTCA
	R: CCAACTTGGTCAATGGAGAA
chrX:35912538-35912753	F: TGAGTCCGAAATTGGAGAGG
	R: GGGAGAAGCCAGCAGGTAT
chrX:36812497-36812710	F: TCAGCCATGAGAATGATCCA
	R: TCCACTGAGAAAGCACTGAAGA
chrX:37431692-37432064	F: AGGAGGTAAGAGGTAGCCCG
	R: GCCTCAGCTTTTGACAGCAG
chrX:38512792-38513002	F: AGTTTTCCATGTGTTTGTCAAGCT
	R: TCCCCTCCTTCAAGCAGGTA

Table S3. Primers Used for Mouse *Cfap47* Genotyping

Primer Names	Primer Sequences (5'-3')	Tm
M-*Cfap47*-F	CCTTGTCTTGTAAACATCTG	60 ℃
M-*Cfap47*-R	GTATGCTTTTATGGTTCAGT	

Table S4. Primers Used for RT-qPCR and RT-PCR Assays

Primer Names	Primer Sequences (5'-3')	Tm
H-*CFAP47*-F	TTTTCATACGTGATTCTACC	60 ℃
H-*CFAP47*-R	TCAAGTGTTACTGGCTGGAC	
H-*GAPDH*-F	GGAGCGAGATCCCTCCAAAAT	60 ℃
H-*GAPDH*-R	GGCTGTTGTCATACTTCTCATGG	
M-*Cfap47*-F	CCAAGTAGTGGTATAGTAAAGG	60 ℃
M-*Cfap47*-R	CATGTGAAACAATTCGATGA	
M-*Gapdh*-F	AGGTCGGTGTGAACGGATTTG	60 ℃
M-*Gapdh*-R	TGTAGACCATGTAGTTGAGGTCA	
M-*Hprt*-F	TGGATATGCCCTTGACTATAATGAG	58 ℃
M-*Hprt*-R	TGGCAACATCAACAGGACTC	

Table S5. Predicted Effects of *CFAP47* Missense Variants on CFAP47 Protein According to the Online Tool HOPE and the Conservation Analysis at UCSC Genome Browser.

	M1	**M2**	**M3**
CFAP47 alteration	**p.Ile2385Asn**	**p.Ser1742Gly**	**p.Pro2890Thr**
Structure	The wild-type residue is predicted to be located in a β-strand while the mutant residue prefers to be in another secondary structure, therefore the local conformation will be slightly destabilized.	The mutation introduces a glycine at this position. Glycines are very flexible and can disturb the required rigidity of the protein at this position.	Prolines are known to be very rigid and therefore induce a special backbone conformation which might be required at this position. The mutation can disturb this special conformation.
Amino acid properties	1) The mutant residue Asparagine is bigger, which might lead to bumps. 2) Hydrophobic interactions will be lost.	1) The wild-type and mutant amino acids differ in size. 2) The mutant residue is smaller, this might lead to loss of interactions.	1) Hydrophobic interactions will be lost. 2) The mutant residue changes a proline into another residue, thereby disturbing the local structure.
Conservation	Highly conserved	Highly conserved	Highly conserved

Table S6. Semen Characteristics and Sperm Morphology in *Cfap47*-Mutated Male Mice

	Wild Type[a]	***Cfap47*$^{-}$/Y**[a]
Semen Parameter[b]		
Sperm concentration (10^6/mL)	23.6 (15.3-31.4)	21.6 (18.3-30.4)
Motility (%)	**74.7 (69.3-80.4)**	**47.8 (28.6-65.2)*** **
Progressive motility (%)	**57.8 (51.9-65.9)**	**29.1 (15.8-39.6)*** **
Sperm Morphology		
Absent flagella (%)	5.0 (1.5-7.0)	13.5 (2.5-15.5)
Short flagella (%)	1.7 (0.5-5.0)	1.2 (0.5-2.5)
Coiled flagella (%)	3.0 (1.5-8.0)	3.4 (1.5-6.5)
Irregular caliber (%)	1.1 (0.5-2.5)	1.3 (0.5-3.0)
Bent flagella (%)	**2.2 (0.5-5.0)**	**15.0 (12.0-18.5)** **

[a] Values represent the mean (range).

[b] Per single epididymis.

** $P < 0.01$, *** $P < 0.001$. The items with statistical significance are shown in bold.